

Hydrogeomorphic Recovery and Temporal Changes in Rainfall Thresholds for Debris Flows Following Wildfire



Special Section:

Fire in the Earth System

Olivia J. Hoch¹ , Luke A. McGuire¹, Ann M. Youberg² , and Francis K. Rengers³ ¹Department of Geosciences, University of Arizona, Tucson, AZ, USA, ²Arizona Geological Survey, University of Arizona, Tucson, AZ, USA, ³U.S. Geological Survey, Golden, CO, USA

Key Points:

- A one-year recurrence interval (RI) storm is sufficient to generate debris flows in the first year following fire
- A 10- to 25-year RI storm may be necessary to initiate a debris flow after two years of recovery
- Temporal changes in debris-flow thresholds are inconsistent across three different burned areas and depend on site-specific recovery trends

Supporting Information:

Supporting Information may be found in the online version of this article.

Correspondence to:

O. J. Hoch,
oliviahoch@email.arizona.edu

Citation:

Hoch, O. J., McGuire, L. A., Youberg, A. M., & Rengers, F. K. (2021). Hydrogeomorphic recovery and temporal changes in rainfall thresholds for debris flows following wildfire. *Journal of Geophysical Research: Earth Surface*, 126, e2021JF006374. <https://doi.org/10.1029/2021JF006374>

Received 26 JUL 2021

Accepted 29 OCT 2021

Abstract Wildfire-induced changes to soil and vegetation promote runoff-generated debris flows in steep watersheds. Postfire debris flows are most commonly observed in steep watersheds during the first wet season following a wildfire, but it is unclear how long the elevated threat of debris flow persists and why debris-flow potential changes in recovering burned areas. This work quantifies how rainfall intensity-duration (ID) thresholds for debris-flow initiation change with time since burning and provides a mechanistic explanation for these changes. We constrained a hydrologic model using field and remotely sensed measurements of soil-infiltration capacity, vegetation cover, runoff, and debris-flow activity. We applied this model to estimate rainfall ID thresholds for debris-flow initiation within three burned areas in the southwestern United States over a postfire recovery period of three to four years. Modeling suggests ID thresholds are lowest immediately following the fire (below a one-year recurrence interval [RI] storm) and increase with time, such that a 10- to 25-year RI storm would be required to generate a debris flow after three years of recovery. Modeled changes in rainfall ID thresholds result from increases in soil infiltration capacity, canopy interception, hydraulic roughness, and median grain size of sediment entrained in an incipient debris flow. The relative importance of each of these factors varied among our three sites. Results improve our ability to assess temporal changes in postfire debris-flow potential, highlight how site-specific factors may alter the persistence of postfire debris-flow hazards, and provide additional constraints on the timescale of recovery following wildfire.

Plain Language Summary Wildfire increases the likelihood of runoff-generated debris flows, which initiate on steep slopes when runoff rapidly erodes sediment, due to fire-induced changes to vegetation cover and soil. The potential for runoff-generated debris flows is greatest in the first year following fire, but less is known about how debris-flow hazards persist through time as the landscape recovers. We assess how debris-flow potential changes through time in three recovering burned areas in the southwestern United States. We estimate changes in the duration and intensity of rainfall required to initiate a debris flow over the first three to four years of recovery at each site. Furthermore, we assess how different aspects of recovery, including vegetation growth and changes in the soil's ability to absorb water, affect the rainfall required for debris-flow initiation. We found that less intense, more frequent rainstorms (occurring every year, on average) were generally capable of producing debris flows in the first year following fire, whereas more intense, less frequent rainstorms (occurring once every 10–25 years, on average) would be necessary after two years of recovery. Results provide constraints on the time period during which there is increased potential for debris-flow hazards downstream of burned areas.

1. Introduction

Wildfires have become more frequent and severe in many different ecosystems and geographic regions, including the western United States (Abatzoglou & Williams, 2016; Singleton et al., 2019; Westerling et al., 2006). Wildfires consume vegetation and litter, decreasing canopy interception (Stoof et al., 2012) and reducing hydraulic roughness (Canfield et al., 2005; Stoof et al., 2015). Fires also can decrease the infiltration capacity of soil relative to unburned areas (DeBano, 2000; Doerr & Moody, 2004; Ebel & Moody, 2017; Larsen et al., 2009; Shakesby & Doerr, 2006). The combination of wildfire-induced changes to soil and vegetation often results in increased runoff and erosion, driven in many cases by infiltration-excess overland flow (Benavides-Solorio & MacDonald, 2001; Moody & Ebel, 2014). In steep watersheds, these fire-induced changes increase the potential for runoff-generated debris flows (Cannon, 2001; Gabet & Bookter, 2008; Kean et al., 2016; Nyman et al., 2011). Debris-flow potential is highest in the first season of rainfall following a wildfire (DeGraff et al., 2015), when debris flows often initiate during relatively frequent (<two-year recurrence interval [RI]) rainstorms (Staley

© 2021. The Authors.

This is an open access article under the terms of the [Creative Commons Attribution-NonCommercial-NoDerivs License](https://creativecommons.org/licenses/by/4.0/), which permits use and distribution in any medium, provided the original work is properly cited, the use is non-commercial and no modifications or adaptations are made.

et al., 2020). As the landscape recovers, the effects of the wildfire become less pronounced, and the potential for runoff-generated debris flows subsides. However, the length of time required for substantial reductions in postfire debris-flow potential and how those potential changes from one environment to another are not well understood.

Rainfall intensity-duration (ID) thresholds, which define a critical rate of rainfall needed over a specified duration to initiate a debris flow, are often used to assess postfire debris-flow likelihood (Staley et al., 2013). Rainfall ID thresholds based on short durations (e.g., 15 min) tend to perform better compared to thresholds based on longer (e.g., >60-min) durations (Kean et al., 2011; Raymond et al., 2020), potentially due to rapid runoff generation via infiltration-excess overland flow in steep, recently burned watersheds (Chen et al., 2013; Ebel, 2020; Schmidt et al., 2011). Rainfall ID thresholds have been empirically developed using past debris flow events to define a rainfall intensity above which debris flows are likely to occur (Cannon et al., 2010; Staley et al., 2013, 2017). To establish reliable thresholds, however, a sufficient number of debris-flow observations and rainfall data are needed to constrain the rainfall intensities that generate debris flows. Because debris flows are most common in the first year following fire (DeGraff et al., 2015) and maintaining debris-flow and rainfall monitoring equipment can be costly and time consuming, a paucity of data constrains the rainfall intensities associated with debris-flow generation in burned areas beyond the first year following a fire. Due to these data limitations, existing empirical rainfall ID thresholds for postfire debris flows are most applicable during the first year following fire.

Runoff-generated debris flows have been observed in response to extreme precipitation events several years after a wildfire (Cannon et al., 2008; Tillery & Rengers, 2020), despite the fact that debris flows are most common during the first year following fire (DeGraff et al., 2015). Cannon et al. (2008) utilized rainfall and flow response observations to determine minimum rainfall thresholds for debris flows and floods immediately following the 2003 Old and Grand Prix Fires in southern California, and after one year of recovery. They found 15-min rainfall ID thresholds increased by ~15 mm/hr after one year of recovery compared to thresholds in the first year following the fire (Cannon et al., 2008). McGuire et al. (2020) used a numerical model, constrained by field measurements made during the initial years of recovery, to estimate temporal changes in rainfall ID thresholds at a site in southern California. Simulations indicated that the 15-min rainfall ID threshold increased from 15–30 mm/hr (<one yr RI) immediately following the fire to 35–40 mm/hr (~one to two yr RI) after one year of recovery and to greater than 60 mm/hr (~10 yr RI) after two years of recovery. At their site in southern California, Thomas et al. (2021) found temporal shifts of simulation-based rainfall ID thresholds of a similar magnitude to Cannon et al. (2008) and McGuire et al. (2020). These studies highlight the short timescale over which rainfall ID thresholds may change in recovering burned areas. However, since timescales for hydrologic recovery can vary greatly from site to site (Ebel & Martin, 2017), the extent to which results translate to other regions is not clear. For example, much of the data used to develop empirical models for postfire debris-flow volume and initiation thresholds in the western U.S. has been collected in the Transverse Ranges in southern California (e.g., Gartner et al., 2014; Staley et al., 2017). Quantifying rates of hydrologic recovery in different environments as well as how those different recovery rates translate into temporal variations in debris-flow potential will help with assessing the extent to which results of these, and similar, postfire debris-flow studies can be generalized across geographic and ecological boundaries.

Soil burn severity (SBS) is one of the key postfire metrics that affects runoff, erosion, and debris-flow generation. SBS describes the impact of the fire on the ground surface including consumption of organic matter, disaggregation of soil structure, and changes to infiltration capacity (Parson et al., 2010). SBS is determined by satellite-derived metrics and adjusted and classified (low, moderate, and high) based on field observations (Parson et al., 2010). Areas burned at moderate and high SBS generally experience more runoff and erosion relative to areas burned at low SBS (Vieira et al., 2015), which in turn can promote debris-flow initiation at lower rainfall intensities (McGuire & Youberg, 2020; Staley et al., 2020). Moderate to high SBS has been identified as a factor that is highly correlated with debris-flow likelihood and volume (Gartner et al., 2014; Staley et al., 2017). The timescale of hydrologic recovery following a fire may also be longer in areas burned at moderate to high SBS, relative to areas burned at low SBS (Ebel et al., 2017). A review of discharge-based recovery times following wildfire found a typical range of two to seven years for hydrologic recovery (Ebel & Martin, 2017). The variability in hydrologic recovery timescale is influenced by the pre-fire landscape characteristics, the magnitude of the fire-induced changes, differing timescales of soil and vegetation recovery, and how changes in soil and vegetation characteristics affect landscape hydrology.

Past studies provide valuable guidance on the typical timescales for soil and vegetation recovery and also highlight expected changes in recovering burned areas that are likely to be important from a hydrogeomorphic perspective. Post-wildfire vegetation recovery, which can influence canopy interception and hydraulic roughness, has been quantified in a variety of environments with differing vegetation types (e.g., Bright et al., 2019; Cerdà & Doerr, 2005; Inbar et al., 1998; Jin et al., 2012; Moreno et al., 2020; Wittenberg et al., 2007). In a seven-year study in southern California, Kinoshita and Hogue (2011) found a reduction in runoff over the period of recovery correlated with measured increases in vegetation. In their study of the 2000 Cerro Grande Fire in northern New Mexico, Canfield et al. (2005) demonstrated that an increase in hydraulic roughness over a three-year period of recovery resulted in a sixfold decrease in peak runoff and a threefold decrease in runoff volume, as well as a factor of 20 decrease in the delivery of sediment from the hillslope to the channel. Rengers, Tucker, et al. (2016) and Tang et al. (2019a) also noted increases in physical and hydraulic roughness during recovery at their study sites in Colorado, USA, and southern California, USA, respectively, which has implications for runoff, erosion, and debris-flow potential (Rengers, Tucker, et al., 2016; Tang et al., 2019a). Soil infiltration capacity is also known to change with time following wildfire (e.g., Ebel & Martin, 2017; Larsen et al., 2009; Robichaud et al., 2016). In a seven-year study in the Colorado Front Range, Ebel (2020) found changes in soil infiltration accounted for a shift in simulated runoff generation from frequent (<1 year RI) storms immediately following fire to only infrequent (more than 30-year RI) storms producing runoff after three years of recovery. Noske et al. (2016) found a reduction in runoff ratio over a five-year period and attributed the reduction to small changes in water repellency and infiltration combined with vegetation regrowth and litter accumulation. Monitoring both temporal changes to soil and vegetation characteristics and runoff/erosion in recovering burned areas helps to provide insights into a causal relationship between recovery of a soil/vegetation characteristic and catchment-scale hydrologic function. Still, it remains unclear how different aspects of recovery contribute to a decrease in the potential for runoff-generated debris flows.

Experiments suggest that runoff-generated debris-flow initiation is related to exceedance of a hydrodynamic threshold (Gregoretti, 2000; Gregoretti & Fontana, 2008; Prancevic et al., 2014), which provides a framework for linking catchment-scale hydrologic recovery to changes in debris-flow potential. Tang et al. (2019b) proposed a slope-dependent dimensionless-discharge threshold for the initiation of runoff-generated debris flows. Using a framework of rainfall-runoff modeling and constraints on parameters relating to soil infiltration capacity, rainfall interception, and grain size of incipient debris flows, a dimensionless-discharge threshold (e.g., Tang et al., 2019b) can be used to determine rainfall ID thresholds for debris-flow initiation (McGuire & Youberg, 2019, 2020; McGuire et al., 2020; Raymond et al., 2020; Tillery & Rengers, 2020). Through constraining the grain size of sediment in likely debris-flow initiation zones and model parameters that govern rainfall-runoff partitioning (i.e., canopy interception, soil infiltration capacity, and hydraulic roughness), a hydrologic model can be used to determine the rainfall intensities and durations required to exceed a dimensionless-discharge threshold.

The primary objectives of this study are to (a) quantify how soil hydraulic properties, canopy interception, and hydraulic roughness change as vegetation and soil recover after a wildfire; (b) use numerical modeling to estimate how rainfall ID thresholds change with time since burning; and (c) provide a physical explanation for why rainfall ID thresholds change with time since burning. In this study, we monitored three different burned areas in the southwestern U.S. (Figure 1) for three or more years to directly assess temporal changes in debris-flow activity and to constrain temporal changes in canopy interception, soil infiltration capacity, hydraulic roughness, and debris-flow grain size during recovery. We use field and remote-sensing data to parameterize a hydrologic model, which we employ to estimate rainfall ID thresholds for generating debris flows as a function of time since burning. We compare modeled ID thresholds with the rainfall intensities that generated debris flows at our study sites. At each site, we focus on temporal changes to areas burned at moderate to high SBS, as these areas are more likely to produce debris flows and therefore pose the greatest risk to communities and infrastructure downstream of burned areas. Quantifying temporal changes in hydrologic response of burned watersheds also provides general insights into the magnitude of fire-induced hydrologic changes and timing of recovery. By understanding which aspects of landscape recovery are most impactful for changing debris-flow initiation thresholds, we will be able to better assess the window of disturbance timescale following a wildfire and apply these findings to similar sites where runoff-generated debris flows are likely.

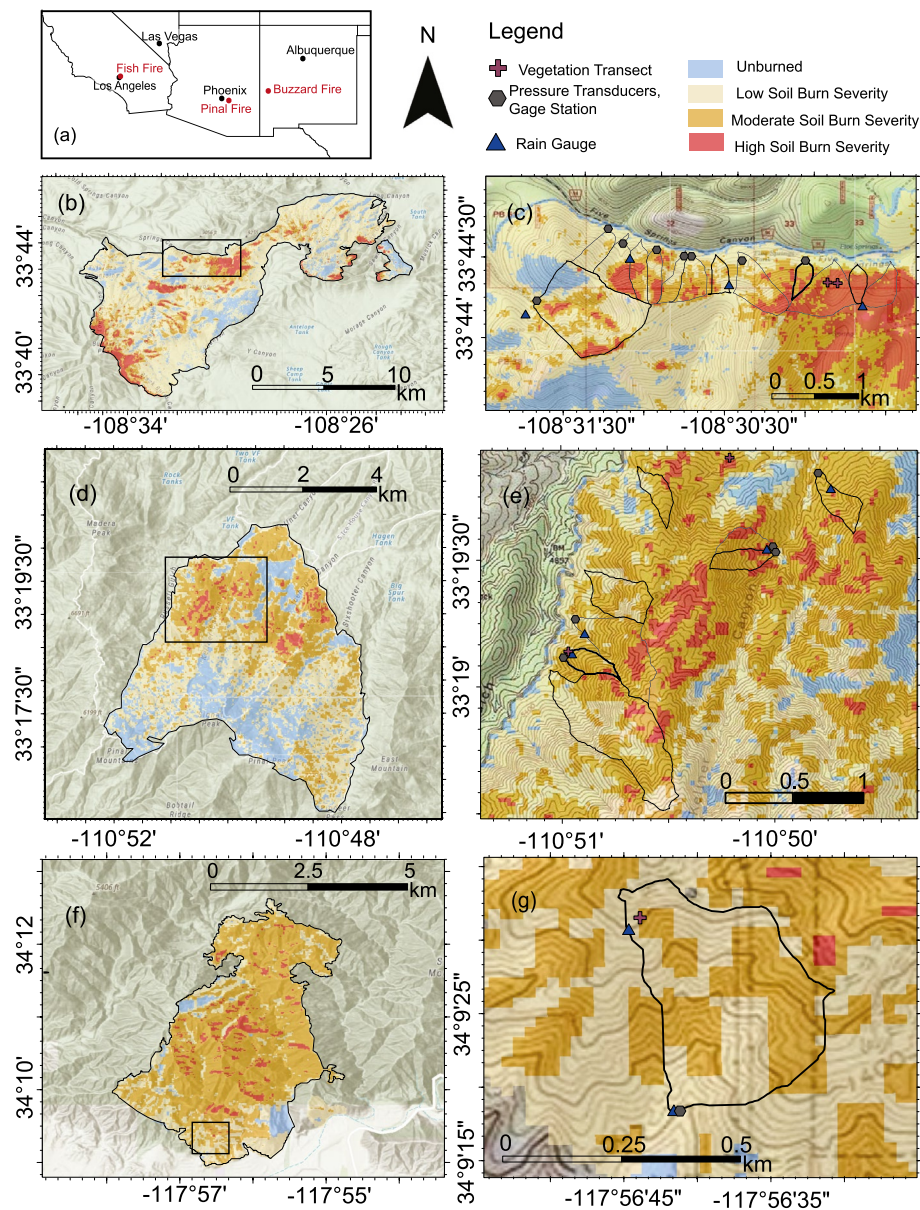


Figure 1. (a) Locations of the three burned study areas in the southwestern United States. Buzzard Fire (b) soil burn severity and hillshade and (c) monitored basins (black outline) with sample and monitoring equipment locations. Pinal Fire (d) soil burn severity and hillshade and (e) monitored basins (black outline) with sample and monitoring equipment locations. Fish Fire (f) soil burn severity and hillshade and (g) monitored basins (black outline) with sample and monitoring equipment locations. The vegetation transect point at the Fish Fire represents the approximate location of all the vegetation transects at this site. Basins used for model calibrations and numerical experiments are indicated by the thick black outline.

2. Study Areas

This study builds on previous work in three study areas in the western U.S.: the 2018 Buzzard Fire in west-central New Mexico, the 2017 Pinal Fire in east-central Arizona, and the 2016 Fish Fire in southern California. Previous studies focused on runoff-generated debris-flow activity in the first year following fire at each site (McGuire & Youberg, 2020; McGuire et al., 2020; Raymond et al., 2020; Tang et al., 2019a) and provide a baseline for the hydrologic and geomorphic conditions immediately following fire that are critical for studying postfire recovery. Below, we provide an overview of each of the three study areas and summarize past work that is most relevant to this study. We combine the findings of these previous studies with new data and observations to examine recovery and debris-flow activity over a period of one to four years postfire, depending on the study area.

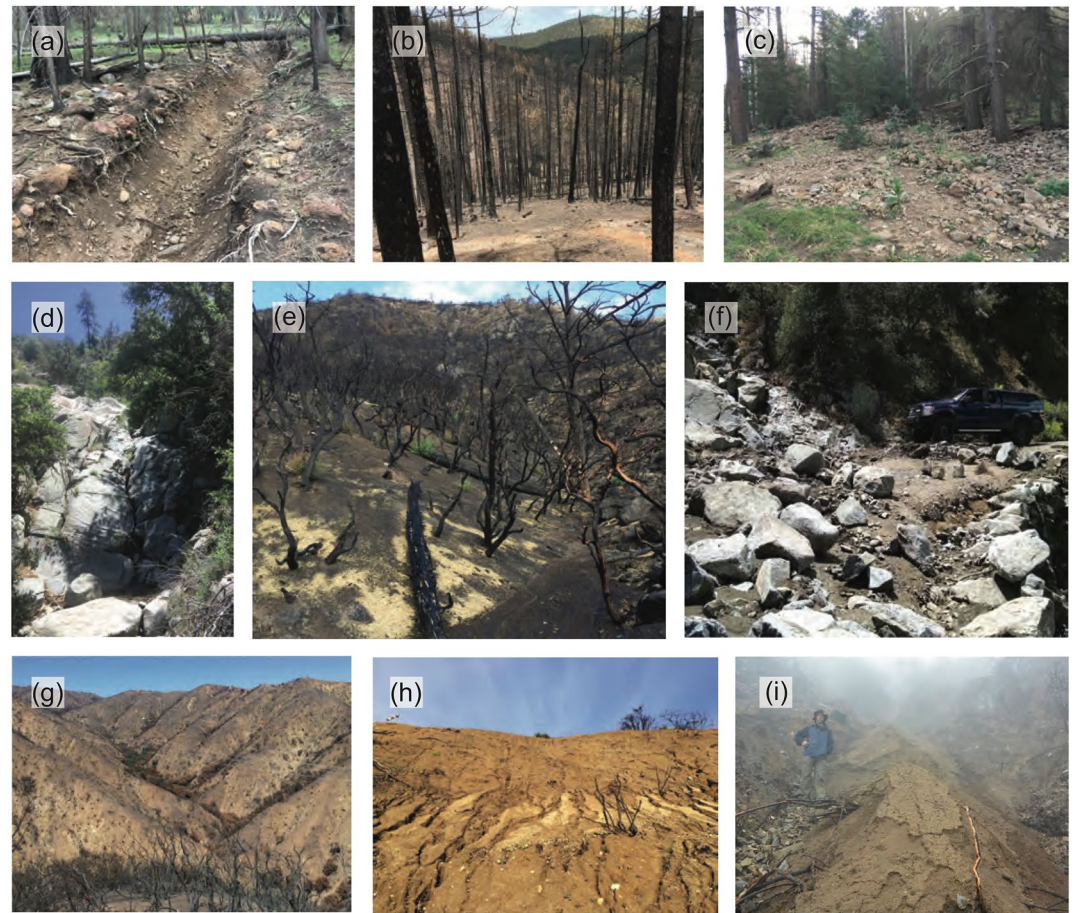


Figure 2. Photos from the Buzzard Fire of (a) a channel scour following an event in year one (June 2020, photo by Olivia Hoch), (b) bare hillslope with minimal vegetation immediately following the fire (July 2018, photo by Luke McGuire), and (c) a debris flow fan deposit (October 2019, photo by Olivia Hoch). Photos from the Pinal Fire of (d) the bedrock channel at the outlet of a basin (May 2020, photo by Olivia Hoch), (e) bare hillslope and channel with minimal vegetation immediately following the fire (July 2017, photo by Luke McGuire), and (f) a debris flow deposit on Forest Road 651 (July 2017, photo by Luke McGuire). Photos from the Fish Fire of (g) the steep, bare hillslopes shortly following the fire (September 2016, photo by Luke McGuire), (h) rilling of a bare hillslope with minimal vegetation several months following the fire (January 2017, photo by Luke McGuire), and (i) dry ravel overlying coarser material in the channel after several rainstorms (January 2017, photo by Francis Rengers).

2.1. Buzzard Fire

In May 2018, the Buzzard Fire burned over 20,000 hectares of the Gila National Forest in the Tularosa Mountains near Reserve, New Mexico (Figure 1). Our study area is underlain by Oligocene basalt-andesite lava flows and tuff (Ratte, 2001), although little bedrock is exposed on hillslopes or in channels. Prior to the fire, eight of 12 study watersheds had an unconfined, soil-mantled swale morphology while four watersheds had defined channels (McGuire & Youberg, 2020) (Figures 2a and 2b). Hillslope soil texture is classified as silt loam (McGuire & Youberg, 2020) and vegetation is primarily ponderosa pine (*Pinus ponderosa*) and Douglas fir (*Pseudotsuga menziesii*). Directly following the fire, negligible amounts of litter, duff, and canopy cover remained in areas burned at moderate to high SBS (McGuire & Youberg, 2020) (Figure 2b). Approximately half of annual rainfall in the region arrives in July, August, and September as a result of the North American Monsoon (Western Regional Climate Center, 2021). The one-year RI 15-min rainfall intensity is ~45 mm/hr and the five-year RI 15-min rainfall intensity is ~75 mm/hr (Bonnin et al., 2011).

McGuire and Youberg (2020) monitored 12 small (<1 km²) watersheds near the northern perimeter of the burned area to determine the characteristics of rainfall that produced debris flows using a combination of three tipping-bucket rain gages, eight in-channel pressure sensors, and four time-triggered cameras. These researchers

also used minidisk tension infiltrometers to estimate soil hydraulic properties within the first several months following the fire and quantified the grain size of debris-flow matrix material within four different debris-flow deposits. McGuire and Youberg (2020) observed 24 debris flows in the first year following the fire (Figure 2c). The debris-flow matrix material had a median grain size (D_{50}) of ~ 0.015 m. The empirically derived 15-min rainfall threshold for triggering a debris flow during the first year following the fire was ~ 42 mm/hr (McGuire & Youberg, 2020).

2.2. Pinal Fire

In May 2017, the Pinal Fire burned over 2,800 hectares of the Tonto National Forest in the Pinal Mountains near Globe in east-central Arizona (Figure 1). The Pinal Mountains are composed of Proterozoic metasedimentary and dioritic intrusive rock, which is exposed in bedrock channels (Richard et al., 2015) (Figure 2d). Hillslope soils texture is classified as a sandy loam (Raymond et al., 2020). The area burned in the Pinal Fire encompasses multiple ecological zones: chaparral vegetation and desert shrub at lower elevations and oak and mixed-conifer forests in the higher elevations. Following the fire, little vegetation remained in the chaparral areas burned at moderate to high SBS (Figure 2e), while some vegetation cover remained in oak and conifer-dominant areas (Raymond et al., 2020). This site receives both winter and summer precipitation, with the summer precipitation coming primarily in July and August as intense rainfall associated with the North American Monsoon. The one-year RI 15-min rainfall intensity is ~ 57 mm/hr and the five-year RI 15-min rainfall intensity is ~ 72 mm/hr (Bonnin et al., 2011).

Raymond et al. (2020) monitored rainfall, runoff, and debris-flow activity in five basins during the first year following the fire (Figure 1e), each of which burned primarily at moderate and high SBS. Eight debris flows were observed in these five watersheds in the first several months following the fire (Figure 2f), and a sample of debris-flow matrix sediment had a D_{50} grain size of 0.0028 m (Raymond et al., 2020). Observations of debris-flow timing, estimated from pressure transducers installed in bedrock channels, and rainfall intensity determined from tipping bucket rain gages, were used to derive an empirical rainfall ID threshold for the first year following the fire. The 15-min rainfall threshold for triggering a debris flow the first year following the Pinal Fire was ~ 56 mm/hr (Raymond et al., 2020). Raymond et al. (2020) also quantified soil hydraulic properties using in situ measurements with minidisk tension infiltrometers, which provided a baseline for comparison with minidisk measurements made in subsequent years during this study. We build off the analyses of Raymond et al. (2020) with additional soil infiltration and vegetation cover measurements and by reporting on additional debris-flow observations from year one in watersheds that were not monitored with pressure transducers.

2.3. Fish Fire

In June 2016, the Fish Fire burned $\sim 1,600$ hectares in the Angeles National Forest in the San Gabriel Mountains (SGM) north of Los Angeles, California (Figure 1). The Fish Fire was part of the San Gabriel Complex, a combination of the Fish and Reservoir Fires. Postfire debris flows have been extensively studied in the SGM (Cannon et al., 2011; DiBiase & Lamb, 2019; Gartner et al., 2014; Kean et al., 2011; McGuire et al., 2017; Palucis et al., 2021; Staley et al., 2014; Tang et al., 2019a). Whereas our focus here is on the Fish Fire, we also include data and model results from past studies that focused on the nearby 2009 Station Fire in order to more effectively parameterize our hydrologic model. Therefore, results from the Fish Fire may be viewed more generally as addressing recovery and changes in debris-flow ID thresholds within the SGM.

The Fish and Station Fire burn scars are located in close proximity and share the same regional climate, vegetation community (chaparral), and topographic characteristics. The SGM are composed primarily of Mesozoic granitic and Proterozoic metamorphic rock (Yerkes & Campbell, 2005), which is exposed on the hillslopes as outcrops or as highly weathered saprolite (Staley et al., 2014). A combination of minimal soil cohesion and steep slopes promotes dry ravel following fire, which loads channels with fine hillslope sediment and helps to fuel debris flow activity (e.g., DiBiase & Lamb, 2019; Florsheim et al., 1991; Lamb et al., 2011). Soils on the hillslopes are generally thin (0.5–1 m), and the textures at our sites are sand to sandy loam (Kean et al., 2011; Tang et al., 2019a). The climate is Mediterranean, consisting of cool wet winters and dry summers. The one-year RI 15-min rainfall intensity is ~ 32 mm/hr, and the five-year RI 15-min rainfall intensity is ~ 53 mm/hr (Perica

et al., 2014). The empirically derived 15-min rainfall intensity for triggering debris flows in the SGM is 19 mm/hr (Staley et al., 2013).

Kean et al. (2011) monitored four low-order watersheds within the Station Fire and observed 23 debris flows in the first year following the fire. The grain-size distribution of debris-flow deposits was determined for four of the debris flows, yielding a range of D_{50} grain sizes from approximately 0.002 to 0.018 m (Kean et al., 2011). The samples from Kean et al. (2011) do not represent the cobble and larger size fractions, and we therefore treat them as being similar to the deposit sampling by McGuire and Youberg (2020) and Raymond et al. (2020) that quantified grain size in the matrix of the deposit. Liu et al. (2021) used the Kineros2 hydrologic model in combination with rain gage and streamflow records to calibrate soil infiltration and hydraulic roughness parameters within a 41.5 km² watershed (burned primarily at moderate-to-high severity) during the first five years following the Station Fire. Liu et al. (2021) found that both saturated hydraulic conductivity and hydraulic roughness in the channel network increased by more than a factor of two over the first several years of recovery. The prior studies by Kean et al. (2011) and Liu et al. (2021) provide valuable information that we use to constrain the hydrologic model for our Fish Fire site.

Our study site within the Fish Fire burn scar, a low-order watershed referred to as Las Lomas, has been the focus of past work, which also benefits the present study. In the first year following the Fish Fire, Tang et al. (2019a) instrumented the Las Lomas watershed (0.12 km²) with a rain gage and a channel monitoring station at the outlet to determine the timing of debris flows and the hydrologic conditions associated with debris-flow initiation (Figure 1g). Negligible amounts of vegetation canopy, litter, or duff remained in this area, and soils were generally water repellent near the surface (McGuire et al., 2019, 2020) (Figures 2g and 2h). Repeat measurements of soil hydraulic properties (from minidisk tension infiltrometers) and canopy/ground cover were collected between September 2016 and March 2019 (one to two years postfire) on portions of a hillslope within this watershed that burned at moderate SBS (McGuire et al., 2019, 2020). Tang et al. (2019a) noted extensive dry ravel deposits in the channel network following the fire (Figure 2i) and observed 11 debris flows at the outlet of this basin during a series of rainstorms between December 2016 and February 2017. There were no runoff-generated debris flows in this watershed during the second postfire wet season (Rengers et al., 2020). In the third wet season following the fire (January 2019), a rainstorm generated more than 200 shallow landslides within the region burned by the Fish Fire (Rengers et al., 2020). No runoff-generated debris flows were generated during this rainstorm (Rengers et al., 2020), despite a peak 15-min rainfall intensity of 53 mm/hr (approximately a five-year RI storm) that greatly exceeded the threshold of 19 mm/hr commonly used in this region to assess debris-flow potential in the first year following fire. We build directly off prior work in the Las Lomas watershed with additional hydrologic model analyses as well as soil infiltration and ground cover measurements.

3. Methods

3.1. Field Measurements

3.1.1. Hydrologic Monitoring

Hydrologic monitoring data collected at our sites were used to assess the rainfall characteristics associated with generating debris flows and in the case of the Pinal and Buzzard Fires, to calibrate a hydrologic model. Since Liu et al. (2021) already calibrated the parameters needed for watershed-scale hydrologic modeling at our Fish Fire site, we did not need to perform additional model calibrations as part of this study. At all three sites, we quantified rainfall using tipping bucket rain gages (Onset RG3-M) (Figure 3a). Runoff and debris-flow activity at the outlet of the Fish Fire site was monitored using a look down laser stage meter (Kean et al., 2019; Tang et al., 2019a). At the Pinal and Buzzard Fire sites, we monitored channel flow at the outlets of several watersheds using unvented pressure transducers (In-Situ Rugged TROLL 100), without a co-located barometric pressure transducer to account for atmospheric effects. The pressure transducers, which were set to take readings at 60 s intervals, were installed in the channel near the basin outlet by drilling a hole in bedrock or a boulder if no bedrock was exposed (Kean et al., 2012; McGuire et al., 2020; McGuire & Youberg, 2020; Raymond et al., 2020) (Figure 3b). At the Buzzard Fire site, pressure transducers were installed at the outlets of six basins in year two and four basins in year three. At the Pinal Fire site, we installed pressure transducers in five basins in year two, four basins in year three, and two basins in year four. We made field observations of flood and debris-flow deposits at basins instrumented with a pressure transducer as well as in basins with no instrumentation in each year (Table S1 in

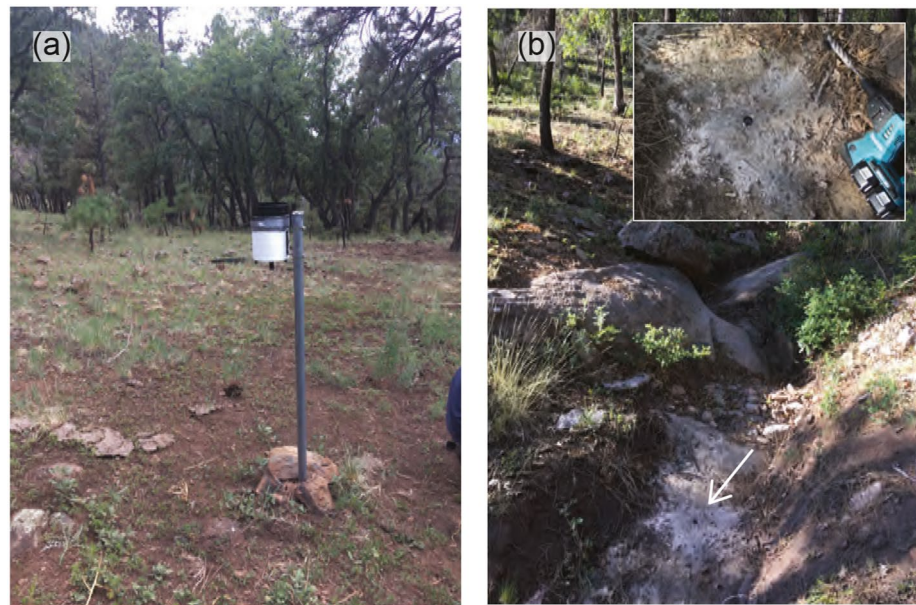


Figure 3. (a) Rain gage at the Buzzard Fire and (b) in-channel pressure transducer at the Buzzard Fire. The arrow indicates the location where we drilled into bedrock and installed the pressure transducer. Inset of installed pressure transducer with drill for scale. Photos by Olivia Hoch.

Supporting Information S1). At each site, postfire year two begins one year following the initiation date of the fire (after one year of recovery), year three begins two years following the initiation date of the fire (after two years of recovery), and year four begins three years following the initiation date of the fire (after 3 years of recovery). The number of watersheds monitored using pressure transducers in each year varied due to equipment availability and site accessibility.

The non-vented pressure transducers used in this study record variations in pressure that may be attributed to changes in flow thickness, flow density, and/or atmospheric pressure. As a result, they are more reliable for quantifying the timing and type of flow (i.e., water-dominated vs. debris-dominated) rather than the absolute magnitude of flow depth. Quantifying the timing of debris flows within rainstorms allows for more accurate determination of the rainfall intensity associated with their initiation, which may vary substantially from the peak rainfall intensity observed during the rainstorm (e.g., McGuire et al., 2021; Raymond et al., 2020; Staley et al., 2013). The passage of debris flows over a pressure transducer often produces a rapid increase in pressure followed by a rapid decrease (Figure 4), whereas the pressure-time series associated with water-dominated flows are typified by more gradual rising and falling limbs (Kean et al., 2012; McGuire & Youberg, 2020; Raymond et al., 2020). In the low-order watersheds ($<1 \text{ km}^2$) monitored here, we assume that the initiation times of debris flows are within tens of minutes prior to the times at which they are observed at the outlet. Therefore, at sites where channel monitoring equipment (pressure transducers) was installed to determine the timing of debris flows at the watershed outlet, we determine the 15-min rainfall intensities (I_{15}) responsible for triggering debris flows using the peak I_{15} recorded within 15 min of when debris flows were observed at the outlet (e.g., Staley et al., 2013). In watersheds that were not instrumented with channel monitoring equipment, the I_{15} associated with debris-flow initiation is taken as the peak I_{15} during the rainstorm. Due to the uncertainty associated with temporal changes in atmospheric pressure, flow density, and erosion, and deposition of sediment on top of the pressure transducers, we also field-verified the occurrence of debris flows based on the presence of characteristic deposits such as the presence of lateral levees along channels and unsorted, matrix-supported deposits (Figure 2c).

In cases where debris flows were relatively undisturbed by post-emplacement flooding, we collected and sieved bulk samples to quantify the D_{50} grain size of debris-flow matrix sediment to estimate the D_{50} grain size of the incipient debris flow. Three debris-flow matrix samples were collected from two deposits at the Buzzard Fire in October 2019 (post-fire year two) and one sample was collected from a deposit at the Pinal Fire in September 2019 (postfire year three). We assessed changes to the debris-flow grain size over time at both sites by comparing

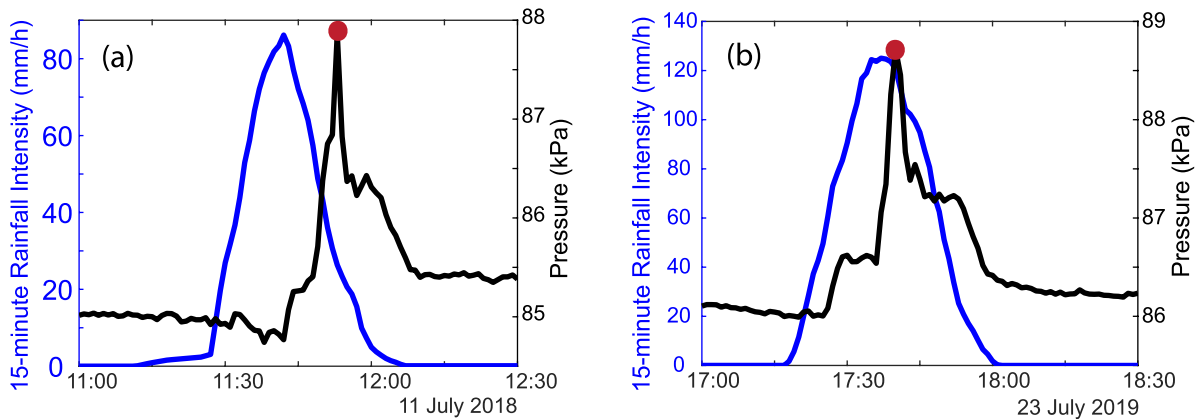


Figure 4. Pressure-transducer data (black line) recording debris flows from the Pinal Fire from (a) Kellner 2 on July 11, 2018 and (b) 651 North on July 23, 2019. The rapid increase in pressure noted by the red circle indicates the time the debris flow passed over the sensor near the watershed outlet. Blue line shows rainfall data recorded by the nearest tipping bucket rain gage.

results of these analyses with the D_{50} grain size of debris-flow matrix sediment reported for the first year following the Buzzard (McGuire & Youberg, 2020) and Pinal (Raymond et al., 2020) Fires.

3.1.2. Soil Hydraulic Properties

In situ measurements to quantify field-saturated hydraulic conductivity (K_s), sorptivity (S), and wetting-front suction head (h_f) were made in postfire years one to three at the Buzzard Fire, years one to four at the Pinal Fire, and years one to four at the Fish Fire (Table S2 in Supporting Information S1) (McGuire et al., 2020; McGuire & Youberg, 2020; Raymond et al., 2020; Tang et al., 2019a). All measurements were made in areas burned at moderate or high SBS using minidisk tension infiltrometers. The infiltrometer has a diameter of 2.25 cm and a suction head set to 1 cm. Data from the in situ measurements were then postprocessed to determine K_s and S following Zhang (1997), who showed $I = C_1\sqrt{t} + C_2t$ where I denotes infiltrated volume, t is time, $C_1 = A_1S$, $C_2 = A_2K_s$, and A_1 and A_2 are empirical coefficients related to soil texture. We determined C_1 and C_2 via three curve-fitting techniques (Vandervaere et al., 2000) and calculated the arithmetic mean of the three values for K_s and S to obtain a single value for K_s and S (following McGuire & Youberg, 2020). We then estimated the wetting front suction head (h_f) according to $h_f = S^2 / (2K_s(\theta_s - \theta_i))$, where θ_s is soil moisture content at saturation, and θ_i is initial soil moisture content. Values of θ_s and θ_i are given in Table S2 in Supporting Information S1 (Carsel & Parrish, 1988; Schaap et al., 2001).

3.1.3. Ground Cover Survey

We conducted ground cover surveys on hillslopes to quantify vegetation cover using the line-point intercept method (Herrick et al., 2009). We established transects on hillslopes in each study area that were a minimum of 20 m in length, running perpendicular to the downslope direction, and noted the surface cover (canopy, litter, soil, or rock fragments) every 0.2 m. Canopy refers to any standing vegetation from the ground surface to eye level. Due to the moderate to high severity of the fire at each of our sites, there was negligible canopy cover at heights greater than eye level. Any loose plant material on the soil surface, including burnt plant material, was classified as litter. Rock fragments were classified as any sediment particles over 5 mm in diameter that were either on the soil surface or embedded in the soil. The timing of measurements at the Buzzard, Pinal, and Fish Fires are reported in Table S3 in Supporting Information S1.

3.2. Remote-Sensing Analysis

Rainfall interception can be modeled using information about vegetation cover and structure (Rutter et al., 1971). One key model parameter, canopy storage capacity, as well as other parameters associated with the rate of drip from the canopy during a rainstorm scale linearly with leaf area (Rutter et al., 1975). We determined the leaf area index (LAI) during each year of recovery at the Buzzard, Pinal, and Fish Fires and used these data in combination with values from existing literature to estimate these infiltration model parameters. Specifically, we used 500-m

LAI data from the Moderate Resolution Imaging Spectroradiometer (MODIS) satellites obtained from the Oak Ridge National Laboratory Distributed Active Archive Center (ORNL DAAC, 2018). LAI is commonly used to assess postfire vegetation recovery (Ebel, 2020; Thomas et al., 2021) and to parameterize rainfall interception models (Thompson et al., 2011). While 500-m data are too coarse to develop basin-specific estimates of interception parameters for the watersheds considered in this study, we use these data to estimate how interception parameters changed over time in areas burned at moderate to high SBS within a particular burn scar.

To estimate a single LAI value for a given year at one of our sites, we averaged the MODIS LAI values within areas burned at moderate to high SBS, as determined by SBS maps produced by the Burned Area Emergency Response teams (USDA Forest Service, 2020) over the season of highest rainfall (and thus greatest likelihood of debris flows). At the Buzzard Fire and the Pinal Fire, we averaged LAI from June 1st to September 1st of each year following the fire, to coincide with the typical timing of monsoon rainfall at those sites. At the Fish Fire, we averaged LAI from December 1st to March 1st of each year to coincide with the winter rainfall that is known to trigger postfire runoff-generated debris flows (Kean et al., 2011; Oakley et al., 2017, 2018). From the composite LAI seasonal average, we averaged all the pixels corresponding with regions burned at moderate to high SBS within the fire perimeter to determine a composite average LAI value that represents the condition of the vegetation in each burned area for each year following the wildfire. This process was also repeated for the five years prior to the fire, which we then averaged at each site to determine a single pre-fire LAI value.

3.3. Numerical Model

We used a process-based numerical model to simulate surface runoff in response to rainfall in select monitored watersheds. The model uses the kinematic wave approximation for overland flow routing and the Green-Ampt equation for infiltration as described in detail by Rengers, McGuire, et al. (2016) and Rengers et al. (2019). We also included the effects of rainfall interception using the framework described in Rutter et al. (1975).

The Green-Ampt equation determines soil infiltration capacity, I_c (m s^{-1}), based on

$$I_c = K_s \left(\frac{Z_f + h_f + h}{Z_f} \right) \quad (1)$$

where Z_f (m), the depth of the wetting front is equal to $V / (\theta_s - \theta_i)$, V (m) is the cumulative infiltrated depth, h (m) is the flow depth, and θ_s and θ_i are dependent on soil texture (Carsel & Parrish, 1988) and denote the volumetric soil moisture content at saturation and the initial soil moisture content, respectively. We represent hydraulic roughness using a depth-dependent Manning coefficient, n ($\text{s m}^{-1/3}$). As flow depth increases, the Manning coefficient approaches a minimum value, n_0 ($\text{s m}^{-1/3}$), as described by the equation

$$n = \begin{cases} n_0 (h/h_c)^{-0.33} & h \leq h_c \\ n_0 & h > h_c \end{cases} \quad (2)$$

where $h_c = 0.003$ m is a critical flow depth above which n becomes constant. The parameter n_0 is calibrated. We constrain n_0 , K_s , and h_f using minidisk measurements, new model calibrations performed during this study, and calibrations performed during previous studies (see Section 3.5).

The Rutter rainfall interception model (Rutter et al., 1975) involves computing the canopy storage, C (m) or volume of water stored in the canopy, per time (t (s)), based on

$$\frac{\partial C}{\partial t} = (1 - T_c)P - D_i \quad (3)$$

where P (m s^{-1}) is the rainfall intensity, and T_c is the throughfall coefficient. The canopy drainage rate (D_i (m s^{-1})) is dependent on the canopy rate coefficient (K_i (m s^{-1})), a decay parameter (g_i (m^{-1})), and the canopy storage capacity (S_i (m)) (Shuttleworth, 1979),

$$D_i = K_i e^{g_i(C - S_i)} \quad (4)$$

The effective rainfall rate, P_{eff} (m s^{-1}), is finally estimated according to

$$P_{\text{eff}} = T_c P + D_i \quad (5)$$

Here, $T_c = 1 - F_c$ where F_c denotes the average fraction vegetation cover measured from vegetation transects in the field. Canopy interception parameters were estimated based on unburned values associated with parameters in similar vegetation types, which we then scaled using remote-sensing-derived LAI to account for the effects of the fire and temporal changes through time. More specifically, S_p , g_p , and K_i were based on values for pine forests and chaparral as reported by Thompson et al. (2011), assuming a linear relationship between LAI and each of these parameters. We scaled S_p , g_p , and K_i at the Pinal Fire and Fish Fire using values estimated for the chaparral-dominant, Sky Oaks site (southern California) reported in Thompson et al. (2011) and scaled S_p , g_p , and K_i at the Buzzard Fire using values estimated from the ponderosa pine-dominant, Metolius site (central Oregon) from Thompson et al. (2011). This parameter estimation method provides a way to parameterize changes in interception that occur through time following a fire while linking those changes to typical values in similar unburned settings.

3.4. Model Calibrations

Since we use the numerical model to estimate rainfall ID thresholds associated with debris flows at each of our sites as a function of time since burning, we need to constrain hydrologic model parameters (n_0 , K_s , h_f) as well as how they change during recovery. In particular, we estimated values of n_0 , K_s , and h_f for each postfire year at each of our three sites.

3.4.1. Buzzard Fire and Pinal Fire

We calibrated the Manning coefficient (n_0) and soil infiltration parameters (K_s and h_f) at the Buzzard and Pinal Fires by comparing runoff data estimated from pressure transducers to simulated hydrographs. To calibrate the model at the Buzzard and Pinal Fires, we iterated through a grid of potential K_s , h_f , and n_0 values and assessed the fit between the modeled and observed runoff response for a selected rainstorm. To improve computational efficiency, we limited the range of potential K_s and h_f values to lie roughly between the first and third quartile of the distributions obtained from the minidisk measurements during the calibration process. We calibrated the model at one basin at the Buzzard Fire and one basin at the Pinal Fire (Figures 1c and 1e) where we had monitoring data for each postfire year (Table S3 in Supporting Information S1).

The pressure-transducer data are best used to quantify flow timing rather than flow depth due to complications associated with varying flow density, atmospheric pressure, and erosion/deposition of sediment on top of the sensor. Therefore, we quantified model performance for a given set of parameters (n_0 , K_s , and h_f) using the difference between the timing of the modeled peak flow discharge and the observed timing of peak pressure recorded at the watershed outlet by the pressure transducer. Flow timing is most influenced by the hydraulic roughness parameter ($n_0 n_0$), while K_s and h_f exert more control over the magnitude of the flow, making it challenging to constrain these two parameters. Therefore, we developed a calibration procedure (using similar approaches to McGuire et al., 2016, 2017; Rengers, McGuire, et al., 2016; Rengers et al., 2019; Tang et al., 2019a, 2019b) that is conservative in terms of the parameter sets that it determines to be inconsistent with the observed pressure data and as described below, we consider uncertainty in calibrated parameters when using the model to estimate debris-flow thresholds. For a given set of parameters, if the difference in peak flow timing between the model and observation was within 15 s and the maximum unit discharge within the channel network was greater than a threshold of 0.10 m²/s that parameter set was retained as a potential fit. Since runoff was observed during each of the calibration rainfall events, we applied a unit discharge threshold to screen out parameter combinations that resulted in adequate agreement in flow timing but negligible runoff. We further refined the selected sets of acceptable parameter combinations in each case by using a second rainstorm from the same year, retaining only those parameter sets that met our criteria for a minimum unit discharge. Rather than identifying a single best-fit value for each parameter, this calibration process resulted in a suite of between 14 and 45 sets of n_0 , K_s , and h_f values that produced acceptable runoff responses for a given site and year since burning (Figure S1 in Supporting Information S1). Since the model requires individual watershed-scale effective values for n_0 , K_s , and h_f we selected a representative set of parameters for each site and each postfire year from the suite of potential fits by choosing the parameter set associated with the median modeled peak discharge. We refer to this set of parameters as the representative parameter values. We used the resulting associated values for n_0 , K_s , and h_f in watershed-scale simulations to explore temporal changes in rainfall ID thresholds.

A model calibration was not possible for year three at the Buzzard Fire and year four at the Pinal Fire since runoff was insufficient to calibrate the model. However, in all other cases, we obtained estimates of K_s and h_f from both minidisk measurements and watershed-scale calibration. We anticipated that the watershed-scale effective values for K_s and h_f may be different from those measured with the minidisk infiltrometers since previous studies have shown that K_s is scale dependent (Ebel et al., 2017; McGuire et al., 2018; Sheridan et al., 2007; Smith and Goodrich, 2000). To assess differences in the value of K_s and h_f due to these two different techniques, we determined the ratio of the median values of the minidisk measurements to the calibrated, watershed-scale parameters for each site as a function of time since burning. The site-specific average of these ratios resulted in a scaling factor for K_s and h_f between point-scale and catchment-scale values. Since we lacked runoff data necessary to calibrate the model at the Buzzard Fire in year three and the Pinal Fire in year four, the scaling factors for these sites were used to estimate the watershed-scale soil hydraulic parameters based on the minidisk measurements. In lieu of runoff data to estimate hydraulic roughness in these two cases, we assumed that roughness (n_0) did not change from the prior year at that site.

3.4.2. Fish Fire

We did not have rainfall and runoff data from the Fish Fire site to calibrate the model for each year following the fire, so we utilized values of K_s and channel Manning's n , which we equate to n_0 , that were calibrated by Liu et al. (2021) for a 41.5 km² watershed that was burned in the nearby 2009 Station Fire. Approximately 83% of the watershed was burned at moderate or high SBS, so we assume that the values calibrated by Liu et al. (2021) reflect conditions in the SGM for areas burned at moderate or high SBS. Liu et al. (2021) determined K_s and Manning's n in the channel network by calibrating the Kineros2 hydrologic model to observed rainfall-runoff responses in the years following the Station Fire. Their analysis provides estimates of K_s and n_0 in postfire years one, two, three, and five. Since values were not calibrated for year four at the Station Fire, we averaged n_0 and K_s in postfire years three and five to estimate year four values for each parameter. As with the Buzzard and Pinal Fires, we compared the watershed-scale K_s values obtained through model calibration with the minidisk-derived K_s at the Fish Fire site for years one to three to provide insight into differences in model parameters that result from spatial scale and measurement technique. Liu et al. (2021) found that the performance of their model was not sensitive to h_f relative to K_s and n_0 , which limited their ability to constrain h_f . Therefore, we utilized the median value of h_f from the minidisk measurements for each postfire year at the Fish Fire in our model simulations associated with that year.

3.5. Numerical Experiments

We determine the I_{15} debris-flow initiation threshold at each site, for each year following the fire, by simulating runoff in response to a series of design rainstorms with different I_{15} . We then evaluated modeled dimensionless discharge throughout the channel network relative to a slope-dependent dimensionless-discharge threshold for debris-flow initiation (Tang et al., 2019b). We selected I_{15} as a metric for the debris flow threshold, as opposed to averaging rainfall over a different duration, because I_{15} is correlated with runoff and debris-flow initiation in small, burned watersheds, and past studies have shown that it performs well as a threshold relative to rainfall intensities averaged over other durations (Kean et al., 2011; Raymond et al., 2020; Staley et al., 2013). Dimensionless discharge is calculated as

$$q^* = \frac{q}{\sqrt{\frac{(\rho_s - \rho)}{\rho} g D_{50}^3}} \quad (6)$$

where gravity (g) is 9.81 m s⁻², sediment density (ρ_s) is 2,600 kg m⁻³, density of the fluid (ρ) is 1,000 kg m⁻³, q is unit discharge (m² s⁻¹), and D_{50} is the median grain size (m) of sediment entrained in an incipient debris flow, which we estimate using the D_{50} of debris flow matrix samples (which excludes cobbles and boulders). We compared the modeled dimensionless discharge to the slope-dependent threshold for debris-flow initiation (Tang et al., 2019b), defined as:

$$q_c^* = \frac{4.29}{\tan \theta^{0.78}} \quad (7)$$

where θ denotes slope.

To determine the I_{15} debris-flow initiation threshold for a particular burn area, we simulated a rainstorm over one of our monitored watersheds with a known I_{15} and compared the peak dimensionless discharge of every channel pixel with the threshold dimensionless discharge, as defined by Equation 7, for that pixel. The simulated storm had a 15-min duration and intensity that was time dependent with a normal distribution (Tang et al., 2019b). If more than half of the channel pixels exceeded the threshold ($q^* > q_c^*$), the I_{15} of the simulated storm was considered to exceed the intensity threshold for debris-flow initiation. If fewer than half of the channel pixels exceeded the dimensionless-discharge threshold, we increased the peak I_{15} of the simulated rainstorm by 5 mm/hr and repeated the process. Channel pixels were defined using a contributing area threshold of 2,000 m² at the Buzzard Fire (McGuire & Youberg, 2020), 500 m² at the Pinal Fire (Raymond et al., 2020), and 1,000 m² at the Fish Fire (Tang et al., 2019b). These thresholds produced channel network extents that were consistent with the presence of gullies and channels based on field observations.

The I_{15} threshold for debris-flow initiation can be expected to vary from one watershed to another within a given burned area, even in cases where SBS is similar, due to differences in topographic slope and variations in channel morphology (McGuire & Youberg, 2020). Here, we are most interested in how rainfall ID thresholds change with time and how those changes are linked with particular aspects of hydrologic recovery. Thus, we take the approach of focusing on a single representative watershed within each burn area. Simulations for estimating the I_{15} threshold were therefore conducted using topography from one of the monitored watersheds within each of the three study areas (Figure 1, Table S4 in Supporting Information S1).

For years one and two at the Buzzard Fire and year one to year three at the Pinal Fire, we determined the model-derived I_{15} debris-flow initiation threshold using the representative parameter values for that year and site. We also determined a model-derived I_{15} debris-flow initiation threshold using calibrated parameters that produced the minimum and maximum discharge from the suite of acceptable parameter combinations to assess the range of likely I_{15} thresholds. Since we lacked similar information on the range of acceptable parameter values in year three at the Buzzard Fire, year four at the Pinal Fire, and years one to four at the Fish Fire, we varied K_s , h_f , and n_o by $\pm 20\%$ to determine the range of likely I_{15} thresholds. For each year at each site, we also varied the D_{50} by $\pm 50\%$ to include the uncertainty in median grain size in the range of likely thresholds.

In addition to determining the I_{15} thresholds, we also used a series of model experiments to determine the extent to which temporal changes in thresholds could be attributed to particular aspects of recovery, namely changes in canopy interception, soil hydraulic properties, hydraulic roughness, and grain size. For each year beyond year one, we simulated recovery under conditions where each parameter that affects dimensionless-discharge calculations (K_s , h_f , n_o , T_c , D_i , D_{50}) remained unchanged from year one. For example, we isolated the importance of soil hydraulic properties on debris-flow initiation thresholds by using the K_s and h_f value from year one in each subsequent year. In this example, all other parameters would change from year to year as appropriate based on observations and calibration. We performed an analogous procedure to determine the relative importance of changes in canopy interception parameters, hydraulic roughness, and D_{50} at each site.

4. Results

4.1. Postfire Recovery

Repeat minidisk infiltrometer measurements and model calibrations at the Buzzard, Pinal, and Fish Fire sites indicate that K_s changed substantially over the three- to four-year period of recovery (Table 1, Figure 5), although the recovery trajectory of K_s varied among sites. At the Buzzard and Fish Fires, the median K_s was lowest the first year following the fire and increased with time since burning according to both the minidisk-derived and calibrated values. At the Pinal Fire, the median K_s was highest the first year following the fire. It then decreased in subsequent years to approximately return to its pre-fire value. The trend in both minidisk and calibrated values of h_f was similar among sites, with h_f being low (< 0.01 m) the first year following the fire and increasing in subsequent years (Table 1, Figure 5).

A Kruskal-Wallis test indicated statistically significant differences ($p < 0.01$) among annual groups of h_f minidisk measurements at each site and among annual groups of K_s minidisk measurements at the Pinal and Buzzard Fires. In cases where the Kruskal-Wallis test indicated statistically significant differences existed, the Wilcoxon rank

Table 1
Summary of Soil Hydraulic Parameters Derived From Minidisk Measurements

Site	Year	Saturated hydraulic conductivity (mm h^{-1})		Wetting front suction head (m)		Number of measurements	Source
		Median	IQR	Median	IQR		
Buzzard Fire	1	7	24	0.0035	0.031	14	McGuire and Youberg (2020)
Buzzard Fire	2	16	12	0.15	0.16	17	This study
Buzzard Fire	3	42	18	0.086	0.108	17	This study
Pinal Fire	1	36	41	0.0035	0.024	20	Raymond et al. (2020)
Pinal Fire	2	45	39	0.03	0.064	26	This study
Pinal Fire	3	21	16	0.052	0.088	15	This study
Pinal Fire	4	15	15	0.031	0.052	13	This study
Fish Fire	1	17	22	0.006	0.021	116	McGuire et al. (2020), Tang et al. (2019a)
Fish Fire	2	21	32	0.021	0.073	21	McGuire et al. (2020)
Fish Fire	3	28	37	0.025	0.049	20	McGuire et al. (2020)
Fish Fire	4	21	14	0.006	0.021	15	This study

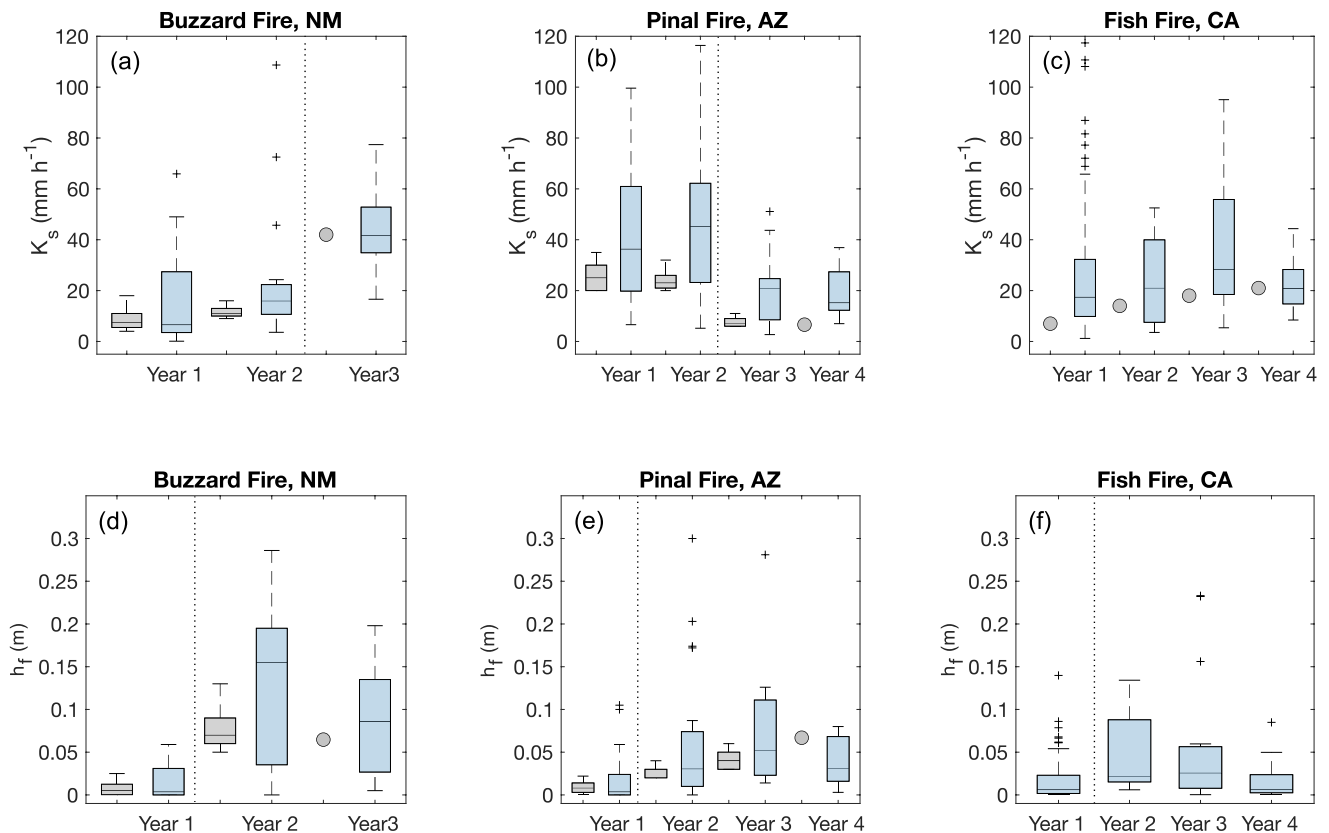


Figure 5. Point-scale minidisk values (light blue) and watershed-scale calibrated values (gray) of saturated hydraulic conductivity for the (a) Buzzard Fire, (b) Pinal Fire, and (c) Fish Fire (San Gabriel Mountains) sites. Point-scale minidisk values (light blue) and watershed calibrated values (gray) of wetting front suction head for the (d) Buzzard Fire and (e) Pinal Fire. Point-scale minidisk values of wetting front suction head for the (f) Fish Fire. Calibrated values for wetting front suction head are not available for the Fish Fire because Liu et al. (2021) found wetting front suction head to have little effect on model performance. Note that two outliers are not visible in panel (b), and four outliers are not visible in panel (c). Minidisk values for year one at the Buzzard Fire are from McGuire and Youberg (2020). Minidisk values for year one at the Pinal Fire are from Raymond et al. (2020). Minidisk values for years one to three at the Fish (San Gabriel Mountains) Fire are from Tang et al. (2019a) and McGuire et al. (2020). Calibrated values used for the Fish Fire (San Gabriel Mountains) are from Liu et al. (2021). The dotted line indicates the timing of significant changes (Wilcoxon rank sum test, $p < 0.01$) in point scale K_s and h_f .

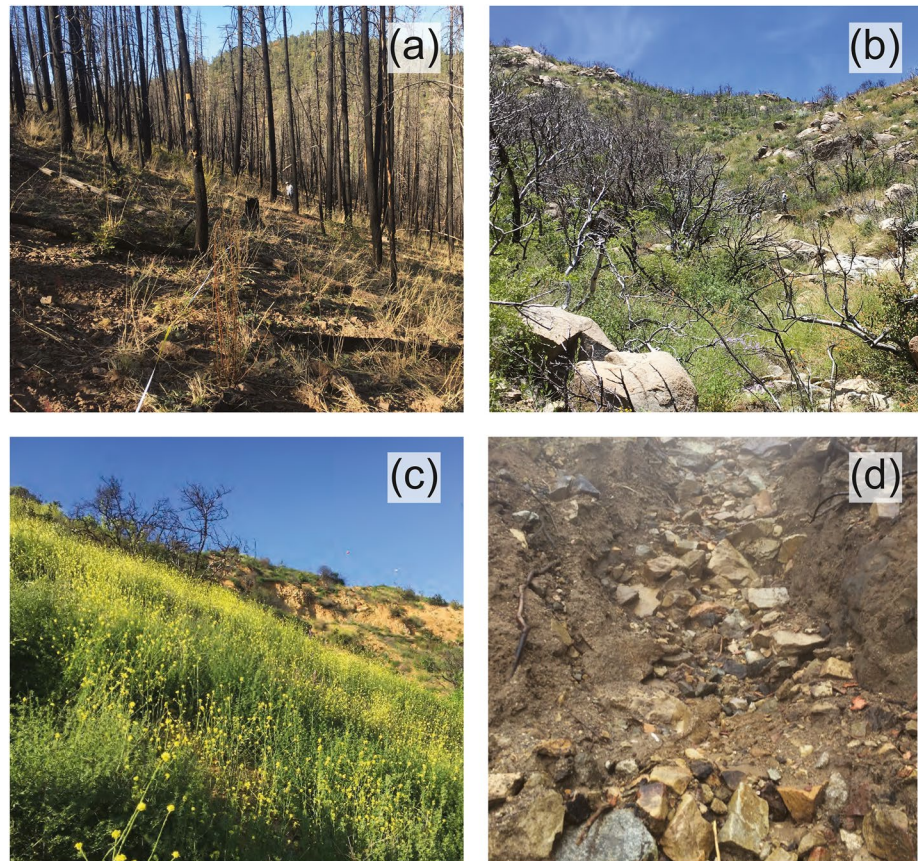


Figure 6. Vegetation on hillslopes during postfire year three at the (a) Buzzard Fire, (b) Pinal Fire, and (c) Fish Fire sites. (d) The channel near the end of the rainy season postfire year one following several floods and debris flows at the Fish Fire where much of the fine sediment, delivered to the channel by postfire dry ravel, has been preferentially eroded (see Figure 2i). Photos by Luke McGuire.

sum test was used to determine when significant changes in soil hydraulic properties occurred by testing for differences from year to year (Figure 5). At each site, the Wilcoxon rank sum test indicated significant changes in minidisk-derived h_f ($p < 0.01$) from postfire year one to year two, but not in subsequent year-to-year changes. At the Buzzard Fire, minidisk-derived K_s did not increase significantly from year one to year two ($p = 0.11$) but did increase significantly from year two to year three ($p < 0.01$). At the Pinal Fire, K_s decreased over the period of recovery, with no significant changes from year one to year two ($p = 0.89$), a significant decrease ($p < 0.01$) from year two to year three, and no significant changes from year three to year four ($p = 0.93$). At the Fish Fire, the Kruskal-Wallis significance test indicated that there was no significant change from year to year in minidisk-derived K_s ($p = 0.14$).

Changes in catchment-scale soil hydraulic properties derived from model calibrations followed a similar trend to the temporal variations indicated by minidisk measurements (Figure 5). However, calibrated parameters that reflect an effective value at the watershed scale were generally smaller than the median of the point-scale minidisk measurements. The average ratio of the median catchment-scale calibrated K_s values to the median point-scale K_s value is 0.92 at the Buzzard Fire, 0.51 at the Pinal Fire, and 0.68 at the Fish Fire site. The site-specific average ratio of the median catchment scale-calibrated values to the median point-scale values of h_f is 0.94 at the Buzzard Fire and 1.24 at the Pinal Fire.

Vegetation cover generally increased over the period of recovery at each site (Figures 2 and 6). The trend in remotely sensed LAI is similar to that of vegetation cover measured at the plot scale (Tables 2 and 3). Calibrated hydraulic roughness also increased from year to year at each site for years where calibration was possible (Table 2). D_{50} grain size at the Pinal and Fish Fires increased from year one while it remained relatively consistent throughout recovery at the Buzzard Fire (Table 2).

Table 2
Summary of Model Parameters Used to Estimate Debris Flow Intensity-Duration Thresholds

Symbol	Definition	Unit	Buzzard Fire			Pinal Fire				Fish Fire			
			Year 1	Year 2	Year 3	Year 1	Year 2	Year 3	Year 4	Year 1	Year 2	Year 3	Year 4
n_0	Hydraulic roughness coefficient	$s\ m^{-1/3}$	0.03	0.05	0.05	0.1	0.2	0.28	0.28	0.09	0.28	0.32	0.3
h_c	Critical depth in roughness model	m	0.003	0.003	0.003	0.003	0.003	0.003	0.003	0.003	0.003	0.003	0.003
ϵ	Exponent in roughness model	–	–0.33	–0.33	–0.33	–0.33	–0.33	–0.33	–0.33	–0.33	–0.33	–0.33	–0.33
K_s	Saturated hydraulic conductivity	$mm\ h^{-1}$	9	12	38	25	27	7	8	7	14	18	21
h_f	Wetting front suction head	m	0.005	0.07	0.08	0.006	0.02	0.05	0.04	0.006	0.021	0.025	0.006
θ_s	Soil moisture at saturation	–	0.45	0.45	0.45	0.41	0.41	0.41	0.41	0.41	0.41	0.41	0.41
θ_i	Initial soil moisture	–	0.067	0.067	0.067	0.065	0.065	0.065	0.065	0.065	0.065	0.065	0.065
g_i	Decay parameter	m^{-1}	2,904	3,402	3,635	1,206	1,192	1,546	1,599	525	938	1,074	1,381
S_i	Canopy storage capacity	mm	1.05	1.23	1.31	1.01	1.0	1.3	1.34	0.44	0.79	0.9	1.16
T_c	Throughfall coefficient	–	1.0	0.61	0.75	1.0	0.77	0.57	0.43	1.0	0.71	0.23	0.05
K_i	Drainage rate coefficient	$m\ s^{-1}$	$1.6 \cdot 10^{-8}$	$3.2 \cdot 10^{-9}$	$1.5 \cdot 10^{-9}$	$4.2 \cdot 10^{-7}$	$4.4 \cdot 10^{-7}$	$7.7 \cdot 10^{-8}$	$5.9 \cdot 10^{-8}$	$1.2 \cdot 10^{-5}$	$1.6 \cdot 10^{-6}$	$8.0 \cdot 10^{-7}$	$1.7 \cdot 10^{-7}$
D_{50}	Median debris flow grain size	m	0.015	0.015	0.015	0.0028	0.022	0.022	0.022	0.008	0.016	0.016	0.016

4.2. Debris-Flow Monitoring

Debris-flow activity dropped off substantially following one year of recovery at all sites. At the Buzzard Fire site, McGuire and Youberg (2020) documented 24 debris flows in year one while we observed two debris flows in year two and no debris flows in year three (Figure 7a, Table 4). Neither year two debris flows occurred in a basin instrumented with a pressure transducer, so the triggering rainfall intensity could not be determined for either of the year two debris flows. At the Pinal Fire, Raymond et al. (2020) documented eight debris flows in postfire year one. We observed one debris flow in year two, which was triggered by an I_{15} of 86 mm/hr, and three debris flows in year three, one of which was triggered by an I_{15} of 117 mm/hr (Figures 4 and 7b and Table 4). The other two debris flows in year three occurred in watersheds where pressure transducers were not installed. At the Fish Fire, no runoff-generated debris flows were observed after the first year (Figure 7c).

Table 3
Summary of Composite MODIS Leaf Area Index (LAI) Values

Site	Recovery year	Mean LAI in moderate/high SBS
Buzzard Fire	Pre-fire	1.46
Buzzard Fire	1	0.71
Buzzard Fire	2	0.83
Buzzard Fire	3	0.89
Pinal Fire	Pre-fire	1.62
Pinal Fire	1	1.09
Pinal Fire	2	1.08
Pinal Fire	3	1.40
Pinal Fire	4	1.45
Fish Fire	Pre-fire	0.91
Fish Fire	1	0.27
Fish Fire	2	0.48
Fish Fire	3	0.55
Fish Fire	4	0.70

Note. Pre-fire values represent a five-year average.

4.3. Modeled Rainfall ID Thresholds for Debris-Flow Initiation

Model-derived rainfall ID thresholds were lowest at each site in the first year following the fire (Figure 7). At the Buzzard Fire, the I_{15} threshold increased from 35 mm/hr in year one (less than one-year RI), to 75 mm/hr in year two (five-year RI), and to 110 mm/hr in year three (25-year RI). At the Pinal Fire, the I_{15} threshold increased from 35 mm/hr (less than one-year RI) in year one to 120 mm/hr (~10-year RI) in year two before leveling off at 115 mm/hr in years three and four. At the Fish Fire, the threshold increased from an I_{15} of 5 mm/hr (less than one-year RI) in year one to 60 mm/hr in year two and then remained relatively constant at 70 mm/hr in year three and 65 mm/hr in year four (~10-year RI) (Figure 7).

Results of our numerical experiments indicate that different factors are responsible for driving temporal changes in rainfall ID thresholds for

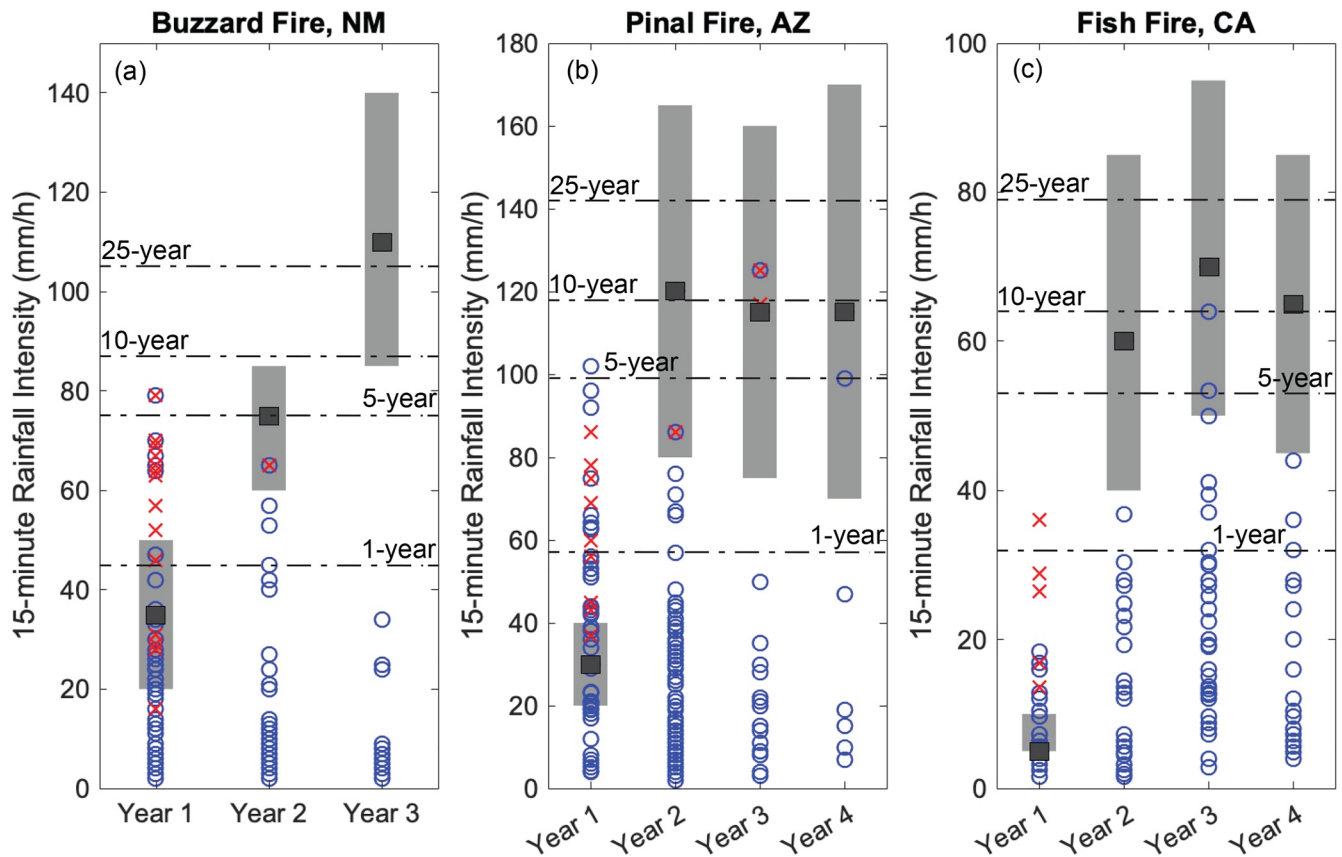


Figure 7. Model estimates of 15-min rainfall thresholds for debris-flow initiation compared to observations of no runoff or floods (blue circles) and debris flows (red crosses). Site-specific rainfall recurrence intervals for I_{15} at the (a) Buzzard Fire, (b) Pinal Fire, and (c) Fish Fire sites are indicated by dashed lines. Dark gray squares represent the threshold based on the representative parameter values at each site. Light gray bars represent the range of thresholds given the range of possible values of soil hydraulic parameters, hydraulic roughness, and D_{50} grain size.

debris-flow initiation at each site (Figure 8). At the Buzzard Fire, the recovery of soil infiltration capacity was of primary importance, with hydraulic roughness and canopy interception influencing thresholds to a lesser extent (Figures 8a and 8d). If temporal changes in soil hydraulic properties were neglected at the Buzzard Fire, the year two ID threshold would be roughly 20 mm/hr lower in year two and 60 mm/hr lower in year three. The D_{50} , however, did not change with time at the Buzzard Fire and therefore played no role in driving temporal changes in the ID threshold. In contrast, at the Pinal Fire, an increase in D_{50} grain size was the largest factor contributing

to modeled increases in the rainfall ID threshold (Figure 8). Recovery of hydraulic roughness and canopy interception also led to temporal increases in the threshold at the Pinal Fire, while changes to soil infiltration capacity, if considered in isolation, would promote decreases in the threshold over time. At the Fish Fire, the recovery of canopy interception was the dominant factor influencing temporal increases in debris-flow initiation thresholds (Figures 8c and 8f). However, recovery of soil infiltration capacity, hydraulic roughness, and D_{50} grain size also contributed to a lesser extent to temporal increases in the modeled threshold.

Table 4
Debris-Flow Observations in Year Two Through Year Four

Site	Year	Catchment ID	Date	Time of debris flow	I_{15} (mm/h)
Buzzard Fire	2	FS94J	August 9, 2019	Unknown	65
Buzzard Fire	2	FS94M	August 9, 2019	Unknown	65
Pinal Fire	2	Kellner 2	July 11, 2018	11:53	86
Pinal Fire	3	651-North	July 7, 2019	17:40	117
Pinal Fire	3	651-C	July 7, 2019	Unknown	125
Pinal Fire	3	651-A	July 7, 2019	Unknown	125

Note. All times listed are local. Catchment ID following McGuire and Youberg (2020) and Raymond et al. (2020).

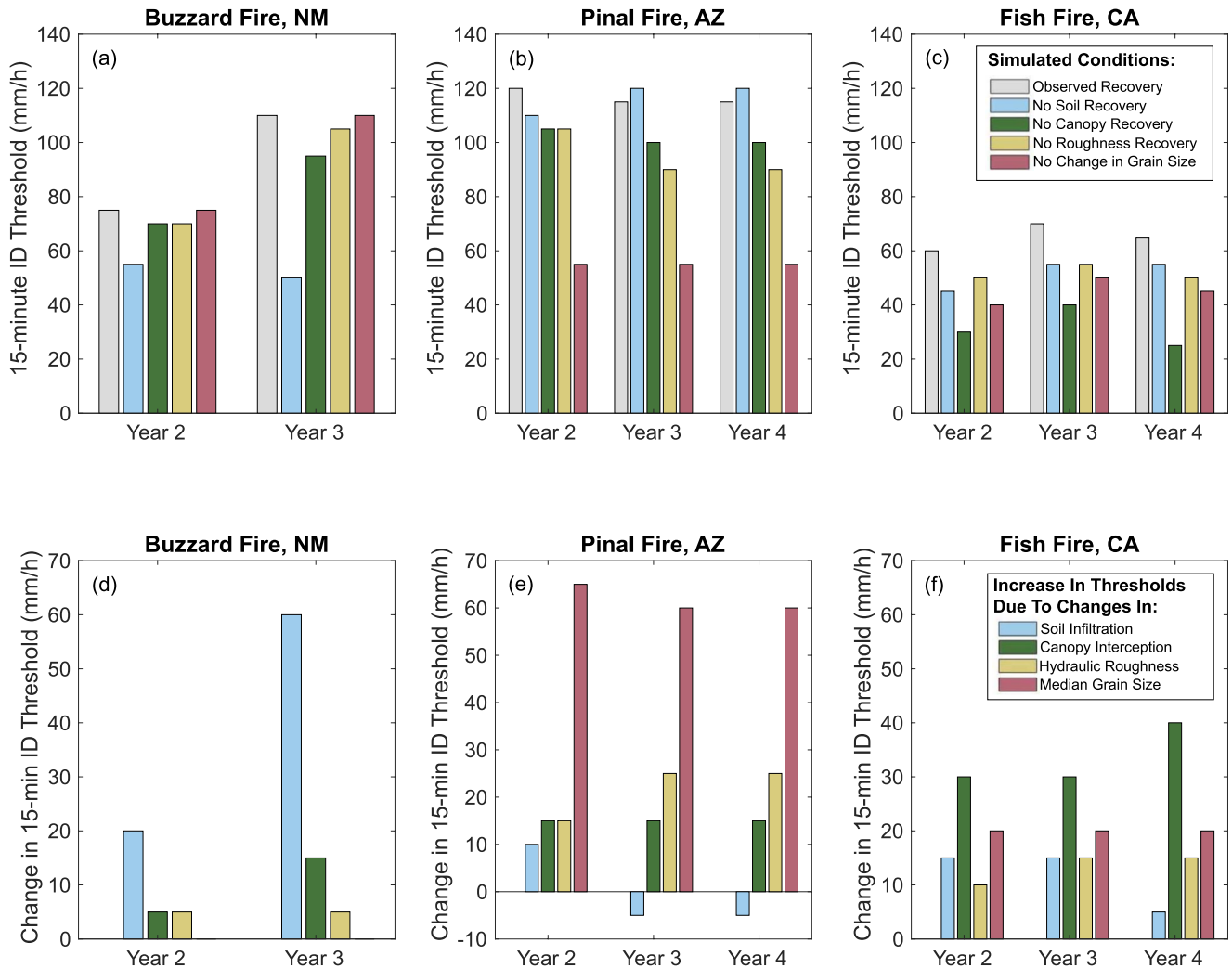


Figure 8. Rainfall intensity-duration (ID) thresholds for debris-flow initiation under the observed recovery conditions and alternate recovery conditions at the (a) Buzzard Fire, (b) Pinal Fire, and (c) Fish Fire sites. The changes in the modeled threshold that results from neglecting particular aspects of recovery (i.e., soil infiltration, canopy interception, hydraulic roughness, or median grain size) are shown on the lower panels for the (d) Buzzard Fire, (e) Pinal Fire, and (f) Fish Fire (San Gabriel Mountains). Legend for panels (a) and (b) are given in panel (c). Legend for panels (d) and (e) are given in panel (f).

5. Discussion

5.1. Postfire Recovery

5.1.1. Soil Infiltration Capacity

Decreases in soil infiltration capacity immediately following wildfire have been widely observed (e.g., Ebel & Moody, 2020; Moody et al., 2013); however, reductions or no change in soil infiltration capacity have also been noted (Doerr et al., 2000; Raymond et al., 2020; Wieting et al., 2017). In many conceptual models of recovery following wildfire, soil infiltration capacity decreases immediately following the fire and then increases monotonically to the pre-fire value (e.g., Ebel & Martin, 2017). Data from the Buzzard Fire are most consistent with this conceptual model. Both the watershed-scale calibrated values for K_s and h_f increase with time since the fire, as do the medians of the minidisk-derived values (Figure 5, Tables 1 and 2). This is also consistent with findings of soil infiltration recovery following a wildfire in an aspen and conifer forest in the Colorado Front Range (Ebel, 2020), in a pinyon-juniper and pine forest in the southwestern U.S. (Canfield et al., 2005), and in a Mediterranean scrubland in Spain (Cerdà, 1998). Minidisk-derived estimates of median K_s at the Fish Fire were lowest in the first postfire year and increased through three years before decreasing again in year four Liu et al. (2021),

however, inferred a consistent increase in K_s from watershed scale calibrations over the first five years of recovery at their nearby site in SGM.

At the Pinal Fire, temporal changes in K_s deviated from the common conceptual model for postfire recovery since K_s decreased with time since burning. In contrast, h_f increased with time at the Pinal Fire (Figure 5, Tables 1 and 2). The general recovery trajectory for both K_s and h_f however, is consistent with a potential return toward unburned values since minidisk measurements from Raymond et al. (2020) showed that K_s was lower and h_f was greater in a nearby unburned area compared with areas burned at moderate to high SBS. This trend may be due to the natural water repellency present in some unburned soils, a property which is common in chaparral ecosystems like those at the Pinal Fire, which may be reduced or destroyed by extreme heating during a fire (DeBano, 1981).

The effect of spatial scale on soil hydraulic properties has been well documented (McGuire et al., 2018; Nyman et al., 2010; Smith & Goodrich, 2000). The average ratio of the median calibrated K_s to median minidisk K_s is below one at each site and median-calibrated h_f to median-minidisk h_f is below one at the Buzzard and Pinal Fires. This indicates the catchment-scale effective K_s and h_f are generally lower than the median of point scale-estimated K_s and h_f values. This result is consistent with previous work on the scale dependence of K_s in recently burned areas (Langhans et al., 2016; McGuire et al., 2018). The ratio of the median-calibrated K_s to median-minidisk K_s is lowest at the Pinal Fire (0.51), intermediate at the Fish Fire (0.68), and highest at the Buzzard Fire (0.92). The lower ratios found at the Pinal and Fish Fires could be related to the presence of exposed bedrock, which may act to decrease the watershed-scale effective values of K_s and h_f . In contrast, bedrock exposure at the Buzzard Fire sites was extremely limited. The variation in ratios of median-calibrated to median-minidisk values may also be attributed to differences in the spatial heterogeneity of soil hydraulic properties among sites. McGuire et al. (2018) found that the watershed-scale effective K_s will tend to be lower, for a given rainfall intensity, in cases where the distribution of spatially variable K_s values has a greater coefficient of variation or where K_s is correlated in space over greater length scales (e.g., due to spatial correlations in fire-enhanced water repellency).

5.1.2. Vegetation

At all three sites, our monitoring period was insufficient to observe complete vegetation recovery. Maximum LAI during the recovery period remained below the pre-fire LAI at each site, suggesting that interception potential also remained below pre-fire levels by the end of the study period. This is consistent with other studies of recovery that utilize remote sensing of vegetation indices and have found that recovery to pre-fire levels takes more than five years (Ebel, 2020; Jin et al., 2012; Kinoshita & Hogue, 2011; Wittenberg et al., 2007). However, the utility of MODIS LAI data may be reduced during the postfire recovery period compared with the pre-fire data, as the postfire vegetation type may be different than the land cover type used for the LAI calculations. Several studies of recovery timing associated with field-based vegetation measurements have found shorter timescales of recovery, with a return to pre-fire conditions in as early as two years (Cerdà & Doerr, 2005; Inbar et al., 1998). The fraction vegetation cover at the Fish and Pinal Fires were both greater than the fraction vegetation cover at the Buzzard Fire in year three (Table 2, Figure 6), potentially due to differences in ecosystem type.

5.1.3. Hydraulic Roughness

Hydraulic roughness was low immediately following the fire and generally increased with time since the fire at our three sites. This is consistent with previous studies showing that physical and/or hydraulic roughness is lowest immediately following the fire and that it increases with time since burning (Canfield et al., 2005; Rengers, Tucker, et al., 2016; Tang et al., 2019a). Liu et al. (2021) found that channel hydraulic roughness returned to pre-fire values by the second year following the Station Fire. While we do not have pre-fire estimates of hydraulic roughness at the Pinal or the Buzzard Fire sites, estimated values for hydraulic roughness remained below those typical of long-unburned forested hillslopes at the Buzzard Fire and above those typical of long-unburned forested hillslopes at the Pinal Fire by the end of the study period (Arcement & Schneider, 1989).

Temporal changes in hydraulic roughness are influenced by changes in ground cover (such as type and amount of vegetation growth) and grain roughness (Rengers, Tucker, et al., 2016; Tang et al., 2019a), and sometimes by channel form roughness related to channel steps (Florsheim et al., 2017; Keller et al., 1997; Rengers et al., 2018). The number and size of runoff-producing storm events also impact hydraulic roughness. As fine sediment is removed from the hillslopes and channels by runoff and debris flows, grain roughness may increase (Figure 2i vs. Figure 6d). For example, a basin that experienced no debris flows in year one, may have a lower year two hydraulic roughness, and therefore a lower rainfall ID threshold, compared with a similar basin that experienced

many debris flows and substantial erosion in year one. Therefore, the expected hydraulic roughness in a recovering burned area is not only dependent on site-specific variables, such as those that affect the rate of revegetation following a fire (i.e., ecosystem type), but also the amount of erosion in previous years. Despite differing amounts of vegetation regrowth and erosion in previous years among our three sites, all sites experienced increases in hydraulic roughness over the period of recovery.

5.1.4. Median Grain Size

Observed changes to D_{50} grain size over the period of recovery varied among sites (Table 2), potentially due to differences in lithology, soil thickness, and sediment transport processes at each site. At the Buzzard Fire, D_{50} grain size remained relatively constant over the period of recovery. However, at the Pinal and Fish Fires, D_{50} grain size was lowest in postfire year one and increased in subsequent years. The D_{50} grain size in postfire year three was roughly 0.022 m, substantially greater than the value of 0.0028 m from year one. We have no debris flow grain size data from postfire year two at the Pinal Fire but hypothesize that the change in debris flow source material resulted from intense rainstorms that produced floods and debris flows in year one, leaving bedrock, cobbles, and boulders exposed throughout much of the channel network. Debris flows at the Buzzard Fire eroded through thick colluvial deposits in many watersheds, sometimes carving gullies greater than 2 m deep without exposing substantial amounts of bedrock (Figure 2a). This suggests that the source material for debris flows at this site did not change over the period of recovery. D_{50} grain size, however, increased by nearly a factor of 10 from year one to year three at the Pinal Fire. Unlike at the Buzzard Fire, bedrock became more regularly exposed over time in the channels at the Pinal Fire site (Figure 2d). This shift indicates that finer material was mobilized by debris flows the first year following the fire and exported from the watershed. In subsequent years, the remaining sediment available for entrainment by debris flows was coarser compared with that of year one. Preferential erosion of fines, both on hillslopes and in channels, as well as sediment redistribution within recently burned watersheds (e.g., Guilinger et al., 2020; Rengers et al., 2021; Staley et al., 2014; Tang et al., 2019a), may play important roles in changing the particle-size distribution of sediment sources for debris flows. The D_{50} grain size of a debris flow from the Fish Fire combined with estimates from Kean et al. (2011) suggest that D_{50} may increase by roughly a factor of two from the first postfire debris flow observed in a watershed to subsequent debris flows (Kean et al., 2011). Dry ravel deposits load channels with relatively fine hillslope sediment following fire in the SGM (DiBiase & Lamb, 2019; Florsheim et al., 1991; Lamb et al., 2011), and as these ravel deposits are eroded, the source sediment for debris flows likely becomes coarser. Reductions in sediment supply within the channel network caused by debris flows and floods in year one at the Fish Fire site may have limited debris-flow activity in subsequent years, especially given that sediment supply from dry ravel plays a large role in fueling postfire debris flows in the SGM (DiBiase & Lamb, 2019).

5.2. Debris-Flow Initiation Thresholds

Results of this study provide insight into how the above-mentioned hydrogeomorphic impacts of fire result in changes to rainfall ID thresholds for debris-flow initiation. Modeled thresholds were lowest in year one and increased over the period of recovery at all three sites. However, simulations indicate that temporal changes in rainfall ID thresholds as well as the reasons for those changes vary among our sites.

5.2.1. Changes in Intensity-Duration Thresholds

Increases in ID thresholds over time were driven primarily by increases in soil infiltration capacity at the Buzzard Fire, increases in D_{50} at the Pinal Fire, and increases in canopy interception at the Fish Fire (Figure 8d). Fire-induced changes to hydraulic roughness, although not quantified as frequently as changes in infiltration capacity in postfire studies, were of similar or greater relative importance compared to changes in infiltration capacity at two of the three sites. Perhaps not surprisingly given links between grain size and hydraulic roughness, the Pinal and Fish Fires sites where changes in hydraulic roughness were more important are also sites where changes in D_{50} were relatively substantial (Figure 8). Results highlight the importance of considering changes in vegetation, roughness, and grain size in addition to infiltration capacity to understand how debris flow potential changes following fire.

The magnitude of the threshold, which is set by the combination of many factors including topography, may also play a role in determining the relative importance of different fire-induced changes on debris-flow potential. Differences in the effect of vegetation recovery on thresholds among our sites, for example, may reflect interactions

between rainfall intensity and canopy interception. A high intensity rainstorm may quickly saturate the canopy storage capacity, making the impact of canopy interception on runoff production negligible during the majority of the rainstorm. However, during a lower intensity rainstorm of the same duration, the canopy may intercept and store a greater proportion of the total rainfall. Since thresholds are lowest at the Fish Fire site, this effect may help explain why canopy interception is of greater relative importance when determining thresholds at that site relative to the Pinal and Buzzard Fire sites. This suggests a potential link between the mechanisms that lead to changes in debris flow potential and the climatology of intense rainfall within that region.

The large range of thresholds (gray bars in Figure 7) represents uncertainty in hydraulic roughness, soil hydraulic properties, and D_{50} grain size. In particular, D_{50} grain size can have a large impact on thresholds and is difficult to constrain due to limited opportunities for sampling. Sampling opportunities are limited by the small number of observed debris flows in latter years and by the tendency for flood flows to partially erode through and redistribute sediment on debris flow deposits. Additional constraints on how the grain-size distribution of debris flow source sediment changes over multiple years of recovery following a fire would benefit our understanding of how debris flow potential changes with time since fire. More generally, changes in overall sediment supply could also play a role. Although we did not quantify sediment supply in this study, the observation of debris flows in year two and beyond at the Buzzard and Pinal Fires indicates that there was enough sediment available in years two and beyond to initiate debris flows if rainstorms were sufficiently intense.

5.2.2. Comparison of Modeled Thresholds to Debris-Flow Observations

Observations of rainfall intensities that triggered debris flows are generally consistent with model-derived estimates of debris-flow initiation thresholds. At the Buzzard Fire, all but one of the observed debris flows were triggered by rainfall with an I_{15} within or above the range of the model thresholds. In the first year following the fire, the modeled rainfall ID threshold ranged from 20 to 50 mm/hr, and one debris flow was triggered by an I_{15} of 16 mm/hr (McGuire & Youberg, 2020). At both the Pinal and Fish Fires, all debris flows were triggered by rainfall with an I_{15} within or above the range of the model thresholds.

The site-specific, empirical threshold for debris-flow initiation in the first year following the Buzzard Fire ($I_{15} = 42$ mm/hr), which was derived by McGuire and Youberg (2020) based on observations of debris-flow occurrence and the corresponding rainfall intensity, is within the range of our numerical model-estimated thresholds for year one (20–50 mm/hr). The empirical threshold for the Pinal Fire ($I_{15} = 56$ mm/hr) (Raymond et al., 2020) is greater than the upper limit of the numerical model thresholds for year one ($I_{15} = 40$ mm/hr). The same is true for the Fish Fire where the empirical threshold for the SGM is $I_{15} = 19$ mm/hr (Staley et al., 2013); and the upper limit of the numerical model-estimated thresholds for year one at the Fish Fire is $I_{15} = 5$ mm/hr. One reason why modeled thresholds may be low relative to empirical thresholds at the Pinal and Fish Fire sites is that the model analyses are performed on a single watershed at each site and assume the entire watershed is burned at moderate or high SBS while empirical thresholds are derived from data from numerous watersheds with more complex SBS patterns. The latter assumption was made since areas burned at moderate and high SBS are more likely to produce debris flows, therefore posing a greater threat to downstream communities and because field measurements of vegetation and soil hydraulic properties were made in moderate to high SBS areas. Wildfires, however, often create a mosaic of SBS and there may be moderate/high SBS, low SBS, and unburned patches within a single watershed. Since hydrologic and geomorphic impacts of fire often scale with SBS (e.g., Moody et al., 2015), we expect the ID threshold to be greater in watersheds where some portion of drainage area was burned at low SBS. Empirical thresholds are also based on data collected during rainstorms with a wide range of durations and total rainfall depths (even for the same or similar peak I_{15}), whereas we estimate ID thresholds using a design storm with a fixed duration.

The reduction in debris-flow occurrence at each site following the first year of recovery is due to a combination of higher rainfall ID thresholds for debris-flow initiation and temporal variability in rainfall intensities that are above the initiation thresholds at our sites (Figure 7). For example, the most intense rainstorm ($I_{15} = 34$ mm/hr) during year three at the Buzzard Fire had less than a one-year RI, whereas there were several instances in postfire year one where rainstorms had greater than a one-year RI. The lack of debris flows during year three at the Buzzard Fire may therefore be attributed to landscape recovery that increased the debris-flow initiation threshold as well as a general lack of intense rainfall. The relatively small number of debris-flow occurrences beyond year one at all three sites highlights the difficulties of using empirical methods to determine rainfall ID thresholds beyond

the first year of postfire recovery. It also illustrates the utility of the modeling approach employed here, which can generate estimates of ID thresholds even in the absence of observed debris flows.

5.3. Implications for Postfire Hazards

Modeling indicates that the RI of rainstorms capable of triggering debris flows varied substantially from site to site and with time since the wildfire. Thresholds tended to be lower at the Fish Fire relative to the Pinal and Buzzard Fires. The one-year RI rainstorm has the lowest I_{15} at the Fish Fire and is greater at the Pinal and Buzzard Fires, suggesting a potential link between the climatology of intense rainfall and thresholds for postfire debris flows (e.g., Cavagnaro et al., 2020). The change in thresholds from year one to two was greater than the change in threshold among subsequent years at each of our three sites, indicating that the greatest reduction in debris flow likelihood takes place between year one and two. A one-year RI rainstorm was sufficient to initiate debris flows at each site immediately following fire, despite substantial differences in the magnitude of the thresholds from site to site. This is consistent with findings from Staley et al. (2020), who found that postfire debris flows were generally associated with one year or less RI rainfall in the southwestern United States the first year following a fire. In the second year following the fire, modeling suggests that a 5- to 10-year RI rainstorm was needed to generate debris flows at each site. By the third year after a fire, 5- to 10-year RI rainstorms may still be sufficient to generate debris flows at two of our sites, while a roughly 25-year RI storm would be needed at the third site. The reduction in debris flow potential by year three was notably lower at our three sites than that found by Ebel (2020) in the Colorado Front Range, who inferred that after three years of recovery, rainfall events with recurrence intervals for I_{15} and I_{30} ranging from 30 to 100 years were required to produce infiltration-excess runoff.

Importantly, not a single aspect of postfire landscape change controls a reduction in debris flow potential for all sites. Recovery of different attributes of the landscape were the primary factor in changing thresholds at each site. The largest impact on thresholds at the Buzzard, Pinal, and Fish Fires were changes to soil infiltration capacity, D_{50} grain size, and canopy interception, respectively. These findings illustrate the degree to which recovery trajectories may vary among burned areas in different environments and highlight the need to consider site- or ecoregion-specific approaches when assessing postfire hydrologic recovery and temporal changes in debris flow hazards. While recovery of soil hydraulic properties and water repellency are often emphasized in recovering burned areas, we found that hydraulic roughness and canopy interception consistently increased with time at all three sites while the same was not always true of parameters governing soil infiltration capacity. Further research is needed in a greater variety of environments across climatic, lithologic, and ecosystem gradients to understand how and why rainfall ID thresholds for debris-flow initiation change throughout the period of recovery. Additionally, as temporal changes in soil, vegetation, roughness, and grain size likely depend on the frequency and intensity of postfire rainfall, further studies of sites similar to the three presented here would illuminate the potential variability in recovery trajectories in similar sites.

6. Conclusion

This work quantifies how rainfall ID thresholds for debris-flow initiation change with time since burning and provides a mechanistic explanation for those changes. During the first season of rainfall following wildfire, the rainfall ID threshold at each site was below the one-year RI rainstorm. By the end of the monitoring period, the rainfall ID threshold was between a 10 and 25-year RI storm at each site. We used a model to quantify differences in the effect of temporal changes in several landscape characteristics (i.e., soil infiltration capacity, canopy interception, hydraulic roughness, and D_{50} grain size) on rainfall ID thresholds for debris-flow initiation. We were not able to identify a single aspect of postfire recovery that controls the reduction in debris flow potential for all sites, indicating that changes in soil infiltration capacity, canopy interception, hydraulic roughness, and D_{50} grain size can all play a role in decreasing runoff generation and debris flow potential in recovering burned areas. Temporal changes in soil infiltration capacity, D_{50} grain size, and canopy interception were the primary factors leading to increases in debris-flow initiation thresholds at the Buzzard Fire, Pinal Fire, and Fish Fire, respectively. Results from this study improve our ability to assess temporal changes in postfire debris flow potential and provide additional constraints on the timescale for recovery following wildfire.

Data Availability Statement

The numerical model (KWAVE) used to simulate runoff is available through the Community Surface Dynamics Modeling System (CSDMS) model repository via <https://csdms.colorado.edu/wiki/Model:KWAVE>. The monitoring data and a summary of the model calibrations are available at HydroShare via <http://www.hydroshare.org/resource/96351adbdacc45e793d8fb5a740d8ac4>.

Acknowledgments

We thank Editor Amy East, one anonymous reviewer, and Don Lindsay for helpful comments that improved the quality of the manuscript. This study was funded in part by the National Integrated Drought Information System (NIDIS) through Task Order 1332KP20FN-RMT0012 and by the U.S. Geological Survey Landslide Hazards Program. We gratefully acknowledge Kelsha Anderson (U.S. Forest Service) for her help providing access to the Angeles National Forest. Any use of trade, firm, or product names is for descriptive purposes only and does not imply endorsement by the U.S. Government.

References

- Abatzoglou, J. T., & Williams, A. P. (2016). Impact of anthropogenic climate change on wildfire across western US forests. *Proceedings of the National Academy of Sciences of the United States of America*, 113(42), 11770–11775. <https://doi.org/10.1073/pnas.1607171113>
- Arcement, G. J., & Schneider, V. R. (1989). Guide for selecting Manning's roughness coefficients for natural channels and flood plains. *U.S. Geological Survey Water Supply Paper*, 2339, 44. <https://doi.org/10.3133/wsp2339>
- Benavides-Solorio, J., & MacDonald, L. H. (2001). Post-fire runoff and erosion from simulated rainfall on small plots, Colorado Front Range. *Hydrological Processes*, 15(15), 2931–2952. <https://doi.org/10.1002/hyp.383>
- Bonnin, G. M., Martin, D., Lin, B., Parzybok, T., Yekta, M., & Riley, D. (2011). NOAA Atlas 14: Precipitation-frequency Atlas of the United States. Volume 1 version 5.0: Semiarid southwest (Arizona, southeast California, Nevada, New Mexico, Utah) (p. 265). *National Oceanic and Administrative Association*. Retrieved from https://www.weather.gov/media/owp/oh/hdsc/docs/Atlas14_Volume1.pdf
- Bright, B. C., Hudak, A. T., Kennedy, R. E., Braaten, J. D., & Henareh Khalyani, A. (2019). Examining post-fire vegetation recovery with Landsat time series analysis in three western North American forest types. *Fire Ecology*, 15(1), 8. <https://doi.org/10.1186/s42408-018-0021-9>
- Canfield, H. E., Goodrich, D. C., & Burns, I. S. (2005). Selection of parameters values to model post-fire runoff and sediment transport at the watershed scale in southwestern forests. In *Managing watersheds for human and natural impacts* (pp. 1–12). American Society of Civil Engineers. [https://doi.org/10.1061/40763\(178\)48](https://doi.org/10.1061/40763(178)48)
- Cannon, S. (2001). Debris flow generation from recently burned watersheds. *Environmental and Engineering Geoscience*, 7(4), 321–341. <https://doi.org/10.2113/gsegeosci.7.4.321>
- Cannon, S., Boldt, E., Laber, J., Kean, J., & Staley, D. (2011). Rainfall intensity–duration thresholds for postfire debris flow emergency-response planning. *Natural Hazards*, 59, 209–236. <https://doi.org/10.1007/s11069-011-9747-2>
- Cannon, S. H., Gartner, J. E., Rupert, M. G., Michael, J. A., Rea, A. H., & Parrett, C. (2010). Predicting the probability and volume of postwildfire debris flows in the intermountain western United States. *Geological Society of America Bulletin*, 122(1–2), 127–144. <https://doi.org/10.1130/B26459.1>
- Cannon, S. H., Gartner, J. E., Wilson, R. C., Bowers, J. C., & Laber, J. L. (2008). Storm rainfall conditions for floods and debris flows from recently burned areas in southwestern Colorado and southern California. *Geomorphology*, 96(3), 250–269. <https://doi.org/10.1016/j.geomorph.2007.03.019>
- Carsel, R. F., & Parrish, R. S. (1988). Developing joint probability distributions of soil water retention characteristics. *Water Resources Research*, 24(5), 755–769. <https://doi.org/10.1029/WR024i005p00755>
- Cavagnaro, D., Delgado, N., McCoy, S. W., Lindsay, D., McGuire, L., Oakley, N., & Lancaster, J. (2020). *Rainfall-intensity thresholds for post-wildfire debris-flow initiation vary with climatology of extreme rainfall*. Abstract NH001-0008 presented at 2020 AGU Fall Meeting, 1–17 Dec.
- Cerdà, A. (1998). Changes in overland flow and infiltration after a rangeland fire in a Mediterranean scrubland. *Hydrological Processes*, 12(7), 1031–1042. [https://doi.org/10.1002/\(SICI\)1099-1085\(19980615\)12:7<1031::AID-HYP636>3.0.CO;2-V](https://doi.org/10.1002/(SICI)1099-1085(19980615)12:7<1031::AID-HYP636>3.0.CO;2-V)
- Cerdà, A., & Doerr, S. H. (2005). Influence of vegetation recovery on soil hydrology and erodibility following fire: An eleven-year investigation. *International Journal of Wildland Fire*, 14(4), 423–437. <https://doi.org/10.1071/WF05044>
- Chen, L., Berli, M., & Chief, K. (2013). Examining modeling approaches for the rainfall-runoff process in wildfire-affected watersheds: Using San Dimas experimental forest. *JAWRA Journal of the American Water Resources Association*, 49(4), 851–866. <https://doi.org/10.1111/jawr.12043>
- DeBano, L. F. (1981). *Water repellent soils: a state-of-the-art* (No. PSW-GTR-46), p. PSW-GTR-46. U.S. Department of Agriculture, Forest Service, Pacific Southwest Forest and Range Experiment Station. <https://doi.org/10.2737/PSW-GTR-46>
- DeBano, L. F. (2000). The role of fire and soil heating on water repellency in wildland environments: A review. *Journal of Hydrology*, 231–232, 195–206. [https://doi.org/10.1016/S0022-1694\(00\)00194-3](https://doi.org/10.1016/S0022-1694(00)00194-3)
- DeGraff, J. V., Cannon, S. H., & Gartner, J. E. (2015). The timing of susceptibility to post-fire debris flows in the western United States. *Environmental & Engineering Geoscience*, 21(4), 277–292. <https://doi.org/10.2113/gsegeosci.21.4.277>
- DiBiase, R. A., & Lamb, M. P. (2019). Dry sediment loading of headwater channels fuels post-wildfire debris flows in bedrock landscapes. *Geology*, 48(2), 189–193. <https://doi.org/10.1130/G46847.1>
- Doerr, S. H., Moody, J. A. (2004). Hydrological effects of soil water repellency: On spatial and temporal uncertainties. *Hydrological Processes*, 18(4), 829–832. <https://doi.org/10.1002/hyp.5518>
- Doerr, S. H., Shakesby, R., & Walsh, R. P. D. (2000). Soil water repellency: Its causes, characteristics and hydro-geomorphological significance. *Earth-Science Reviews*, 51(1–4), 33–65. [https://doi.org/10.1016/S0012-8252\(00\)00011-8](https://doi.org/10.1016/S0012-8252(00)00011-8)
- Ebel, B. A. (2020). Temporal evolution of measured and simulated infiltration following wildfire in the Colorado Front Range, USA: Shifting thresholds of runoff generation and hydrologic hazards. *Journal of Hydrology*, 585, 124765. <https://doi.org/10.1016/j.jhydrol.2020.124765>
- Ebel, B. A., & Martin, D. A. (2017). Meta-analysis of field-saturated hydraulic conductivity recovery following wildland fire: Applications for hydrologic model parameterization and resilience assessment. *Hydrological Processes*, 31(21), 3682–3696. <https://doi.org/10.1002/hyp.11288>
- Ebel, B. A., & Moody, J. A. (2017). Synthesis of soil-hydraulic properties and infiltration timescales in wildfire-affected soils. *Hydrological Processes*, 31(2), 324–340. <https://doi.org/10.1002/hyp.10998>
- Ebel, B. A., & Moody, J. A. (2020). Parameter estimation for multiple post-wildfire hydrologic models. *Hydrological Processes*, 34(21), 4049–4066. <https://doi.org/10.1002/hyp.13865>
- Ebel, B. A., Romero, O. C., & Martin, D. A. (2017). Thresholds and relations for soil-hydraulic and soil-physical properties as a function of burn severity four years after the 2011 Las Conchas Fire, New Mexico, USA. *Hydrological Processes*, 32(14), 2263–2278. <https://doi.org/10.1002/hyp.13167>

- Florsheim, J. L., Chin, A., Kinoshita, A. M., & Nourbakhshbeidokhti, S. (2017). Effect of storms during drought on post-wildfire recovery of channel sediment dynamics and habitat in the southern California chaparral, USA. *Earth Surface Processes and Landforms*, 42(10), 1482–1492. <https://doi.org/10.1002/esp.4117>
- Florsheim, J. L., Keller, E. A., & Best, D. W. (1991). Fluvial sediment transport in response to moderate storm flows following chaparral wildfire, Ventura County, southern California. *Geological Society of America Bulletin*, 103(4), 504–511. [https://doi.org/10.1130/0016-7606\(1991\)103<0504:FSTIRT>2.3.CO;2](https://doi.org/10.1130/0016-7606(1991)103<0504:FSTIRT>2.3.CO;2)
- Gabet, E. J., & Bookter, A. (2008). A morphometric analysis of gullies scoured by post-fire progressively bulked debris flows in southwest Montana, USA. *Geomorphology*, 96(3–4), 298–309. <https://doi.org/10.1016/j.geomorph.2007.03.016>
- Gartner, J. E., Cannon, S. H., & Santi, P. M. (2014). Empirical models for predicting volumes of sediment deposited by debris flows and sediment-laden floods in the transverse ranges of southern California. *Engineering Geology*, 176, 45–56. <https://doi.org/10.1016/j.enggeo.2014.04.008>
- Gregoretti, C. (2000). The initiation of debris flow at high slopes: Experimental results. *Journal of Hydraulic Research*, 38(2), 83–88. <https://doi.org/10.1080/00221680009498343>
- Gregoretti, C., & Fontana, G. D. (2008). The triggering of debris flow due to channel-bed failure in some alpine headwater basins of the Dolomites: Analyses of critical runoff. *Hydrological Processes*, 22(13), 2248–2263. <https://doi.org/10.1002/hyp.6821>
- Guilinger, J. J., Gray, A. B., Barth, N. C., & Fong, B. T. (2020). The evolution of sediment sources over a sequence of post-fire sediment-laden flows revealed through repeat high-resolution change detection. *Journal of Geophysical Research: Earth Surface*, 125(10), e2020JF005527. <https://doi.org/10.1029/2020JF005527>
- Herrick, J. E., Van Zee, J. W., Havstad, K. M., Burkett, L. M., & Whitford, W. G., (Eds.), (2009). *Monitoring manual for grassland, shrubland, and savanna ecosystems volume 1: Quick start*. USDA - ARS Jordana Experimental Range; Distributed by the University of Arizona Press.
- Inbar, M., Tamir, M., & Wittenberg, L. (1998). Runoff and erosion processes after a forest fire in Mount Carmel, a Mediterranean area. *Geomorphology*, 24(1), 17–33. [https://doi.org/10.1016/S0169-555X\(97\)00098-6](https://doi.org/10.1016/S0169-555X(97)00098-6)
- Jin, Y., Randerson, J. T., Goetz, S. J., Beck, P. S. A., Lorant, M. M., & Goulden, M. L. (2012). The influence of burn severity on postfire vegetation recovery and albedo change during early succession in North American boreal forests. *Journal of Geophysical Research*, 117(G1), G01036. <https://doi.org/10.1029/2011JG001886>
- Kean, J. W., McGuire, L. A., Rengers, F. K., Smith, J. B., & Staley, D. M. (2016). Amplification of postwildfire peak flow by debris. *Geophysical Research Letters*, 43(16), 8545–8553. <https://doi.org/10.1002/2016GL069661>
- Kean, J. W., Smith, J. B., Rengers, F. K., McGuire, L. A., & Staley, D. M. (2019). *Post-wildfire debris flow monitoring data, Las Lomas, 2016 fish fire, Los Angeles County, California, November 2016 to February 2017*. U.S. Geological Survey data release. <https://doi.org/10.5066/P9F3YTBP>
- Kean, J. W., Staley, D. M., & Cannon, S. H. (2011). In situ measurements of post-fire debris flows in southern California: Comparisons of the timing and magnitude of 24 debris flow events with rainfall and soil moisture conditions. *Journal of Geophysical Research*, 116(F4), F04019. <https://doi.org/10.1029/2011JF002005>
- Kean, J. W., Staley, D. M., Leeper, R. J., Schmidt, K. M., & Gartner, J. E. (2012). A low-cost method to measure the timing of postfire flash floods and debris flows relative to rainfall. *Water Resources Research*, 48(5), W05516. <https://doi.org/10.1029/2011WR011460>
- Keller, E. A., Valentine, D. W., & Gibbs, D. R. (1997). Hydrological response of small watersheds following the southern California painted cave fire of June 1990. *Hydrological Processes*, 11(4), 401–414. [https://doi.org/10.1002/\(SICI\)1099-1085\(19970330\)11:4<401::AID-HYP447>3.0.CO;2-P](https://doi.org/10.1002/(SICI)1099-1085(19970330)11:4<401::AID-HYP447>3.0.CO;2-P)
- Kinoshita, A. M., & Hogue, T. S. (2011). Spatial and temporal controls on post-fire hydrologic recovery in southern California watersheds. *Catena*, 87(2), 240–252. <https://doi.org/10.1016/j.catena.2011.06.005>
- Lamb, M. P., Scheingross, J. S., Amidon, W. H., Swanson, E., & Limaye, A. (2011). A model for fire-induced sediment yield by dry ravel in steep landscapes. *Journal of Geophysical Research*, 116(F3), F03006. <https://doi.org/10.1029/2010JF001878>
- Langhans, C., Lane, P. N. J., Nyman, P., Noske, P. J., Cawson, J. G., Oono, A., & Sheridan, G. J. (2016). Scale-dependency of effective hydraulic conductivity on fire-affected hillslope. *Water Resources Research*, 52(7), 5041–5055. <https://doi.org/10.1002/2016WR018998>
- Larsen, I. J., Macdonald, L. H., Brown, E., Rough, D., Welsh, M. J., Pietraszek, J. H., et al. (2009). Causes of post-fire runoff and erosion: Water repellency, cover, or soil sealing? *Soil Science Society of America Journal*, 73(4), 1393–1407. <https://doi.org/10.2136/sssaj2007.0432>
- Liu, T., McGuire, L. A., Wei, H., Rengers, F. K., Gupta, H., Ji, L., & Goodrich, D. C. (2021). The timing and magnitude of changes to Hortonian overland flow at the watershed scale during the post-fire recovery process. *Hydrological Processes*, 35(5), e14208. <https://doi.org/10.1002/hyp.14208>
- McGuire, L., Kean, J., Staley, D., Rengers, F., & Wasklewicz, T. (2016). Constraining the relative importance of raindrop- and flow-driven sediment transport mechanisms in post-wildfire environments and implications for recovery time scales. *Journal of Geophysical Research: Earth Surface*, 121, 2211–2237. <https://doi.org/10.1002/2016JF003867>
- McGuire, L. A., Rengers, F. K., Kean, J. W., & Staley, D. M. (2017). Debris flow initiation by runoff in a recently burned basin: Is grain-by-grain sediment bulking or en masse failure to blame? *Geophysical Research Letters*, 44(14), 7310–7319. <https://doi.org/10.1002/2017GL074243>
- McGuire, L. A., Rengers, F. K., Kean, J. W., Staley, D. M., & Mirus, B. B. (2018). Incorporating spatially heterogeneous infiltration capacity into hydrologic models with applications for simulating post-wildfire debris flow initiation. *Hydrological Processes*, 32(9), 1173–1187. <https://doi.org/10.1002/hyp.11458>
- McGuire, L. A., Rengers, F. K., Kean, J. W., Staley, D. M., Tang, H., & Youberg, A. M. (2019). *Looking through the window of disturbance at post-wildfire debris flow hazards*. Seventh International Conference on Debris-Flow Hazards Mitigation, 8 pp. <https://doi.org/10.25676/11124/173177>
- McGuire, L. A., Rengers, F. K., Oakley, N., Kean, J. W., Staley, D. M., Tang, H., et al. (2020). Time since burning and rainfall characteristics impact post-fire debris flow initiation and magnitude. *Environmental and Engineering Geoscience*, 27(1), 43–56. <https://doi.org/10.2113/EEG-D-20-00029>
- McGuire, L. A., & Youberg, A. M. (2019). Impacts of successive wildfire on soil hydraulic properties: Implications for debris flow hazards and system resilience. *Earth Surface Processes and Landforms*, 44(11), 2236–2250. <https://doi.org/10.1002/esp.4632>
- McGuire, L. A., & Youberg, A. M. (2020). What drives spatial variability in rainfall intensity-duration thresholds for post-wildfire debris flows? Insights from the 2018 Buzzard Fire, NM, USA. *Landslides*, 17, 2385–2399. <https://doi.org/10.1007/s10346-020-01470-y>
- McGuire, L. A., Youberg, A. M., Rengers, F. K., Abramson, N. S., Ganesh, I., Gorr, A. N., et al. (2021). Extreme precipitation across adjacent burned and unburned watersheds reveals impacts of low severity wildfire on debris-flow processes. *Journal of Geophysical Research: Earth Surface*, 126(4), e2020JF005997. <https://doi.org/10.1029/2020JF005997>
- Moody, J. A., & Ebel, B. A. (2014). Infiltration and runoff generation processes in fire-affected soils. *Hydrological Processes*, 28(9), 3432–3453. <https://doi.org/10.1002/hyp.9857>

- Moody, J. A., Ebel, B. A., Nyman, P., Martin, D. A., Stooft, C., McKinley, R., et al. (2015). Relations between soil hydraulic properties and burn severity. *International Journal of Wildland Fire*, 25(3), 279–293. <https://doi.org/10.1071/WF14062>
- Moody, J. A., Shakesby, R. A., Robichaud, P. R., Cannon, S. H., & Martin, D. A. (2013). Current research issues related to post-wildfire runoff and erosion processes. *Earth-Science Reviews*, 122, 10–37. <https://doi.org/10.1016/j.earscirev.2013.03.004>
- Moreno, H. A., Gourley, J. J., Pham, T. G., & Spade, D. M. (2020). Utility of satellite-derived burn severity to study short- and long-term effects of wildfire on streamflow at the basin scale. *Journal of Hydrology*, 580, 124244. <https://doi.org/10.1016/j.jhydrol.2019.124244>
- Noske, P. J., Nyman, P., Lane, P. N. J., & Sheridan, G. J. (2016). Effects of aridity in controlling the magnitude of runoff and erosion after wildfire. *Water Resources Research*, 52(6), 4338–4357. <https://doi.org/10.1002/2015WR017611>
- Nyman, P., Sheridan, G., & Lane, P. (2010). Synergistic effects of water repellency and macropore flow on the hydraulic conductivity of a burned forest soil, south-east Australia. *Hydrological Processes*, 24, 2871–2887. <https://doi.org/10.1002/hyp.7701>
- Nyman, P., Sheridan, G. J., Smith, H. G., & Lane, P. N. J. (2011). Evidence of debris flow occurrence after wildfire in upland catchments of south-east Australia. *Geomorphology*, 125(3), 383–401. <https://doi.org/10.1016/j.geomorph.2010.10.016>
- Oakley, N. S., Cannon, F., Munroe, R., Lancaster, J. T., Gomberg, D., & Ralph, F. M. (2018). Brief communication: Meteorological and climatological conditions associated with the 9 January 2018 post-fire debris flows in Montecito and Carpinteria California, USA. *Natural Hazards and Earth System Sciences Discussions*, 18, 3037–3043. <https://doi.org/10.5194/nhess-18-3037-2018>
- Oakley, N. S., Lancaster, J. T., Kaplan, M. L., & Ralph, F. M. (2017). Synoptic conditions associated with cool season post-fire debris flows in the Transverse Ranges of southern California. *Natural Hazards*, 88(1), 327–354. <https://doi.org/10.1007/s11069-017-2867-6>
- ORNL DAAC. (2018). *MODIS and VIIRS land products global subsetting and visualization tool*. ORNL DAAC. <https://doi.org/10.3334/ORNLDAAC/1379>
- Palucis, M. C., Ulizio, T. P., & Lamb, M. P. (2021). Debris flow initiation from ravel-filled channel bed failure following wildfire in a bedrock landscape with limited sediment supply. *Geological Society of America Bulletin*, 133(9–10), 2079–2096. <https://doi.org/10.1130/B35822.1>
- Parson, A., Robichaud, P. R., Lewis, S. A., Napper, C., & Clark, J. T. (2010). *Field guide for mapping post-fire soil burn severity*. (No. RMRS-GTR-243). U.S. Department of Agriculture, Forest Service, Rocky Mountain Research Station. <https://doi.org/10.2737/RMRS-GTR-243>
- Perica, S., Dietz, S., Heim, S., Hiner, L., Maittaria, K., Martin, D., et al. (2014). NOAA Atlas 14: Precipitation-frequency Atlas of the United States. Volume 6 version 2.3: California (p. 233). National Oceanic and Administrative Association. Retrieved from https://www.weather.gov/media/owp/oh/hdsc/docs/Atlas14_Volume6.pdf
- Prancevic, J. P., Lamb, M. P., & Fuller, B. M. (2014). Incipient sediment motion across the river to debris flow transition. *Geology*, 42(3), 191–194. <https://doi.org/10.1130/G34927.1>
- Ratte, J. (2001). *Geologic map of the Tularosa Mountains 30' × 60' quadrangle, Catron County, New Mexico*. U.S. Geological Survey Geologic Investigations Series Map I-2619. <https://doi.org/10.3133/i2619>
- Raymond, C. A., McGuire, L. A., Youberg, A. M., Staley, D. M., & Kean, J. W. (2020). Thresholds for post-wildfire debris flows: Insights from the Pinal Fire, Arizona, USA. *Earth Surface Processes and Landforms*, 45(6), 1349–1360. <https://doi.org/10.1002/esp.4805>
- Rengers, F. K., McGuire, L. A., Ebel, B. A., & Tucker, G. E. (2018). The evolution of a colluvial hollow to a fluvial channel with periodic steps following two transformational disturbances: A wildfire and a historic flood. *Geomorphology*, 309, 121–130. <https://doi.org/10.1016/j.geomorph.2018.01.003>
- Rengers, F. K., McGuire, L. A., Kean, J. W., Staley, D. E., & Hobley, D. E. J. (2016). Model simulations of flood and debris flow timing in steep catchments after wildfire: Simulations of flood and debris flow timing. *Water Resources Research*, 52(8), 6041–6061. <https://doi.org/10.1002/2015WR018176>
- Rengers, F. K., McGuire, L. A., Kean, J. W., Staley, D. M., Dobre, M., Robichaud, P. R., & Swetnam, T. (2021). Movement of sediment through a burned landscape: Sediment volume observations and model comparisons in the San Gabriel Mountains, California, USA. *Journal of Geophysical Research: Earth Surface*, 126(7), e2020JF006053. <https://doi.org/10.1029/2020JF006053>
- Rengers, F. K., McGuire, L. A., Kean, J. W., Staley, D. M., & Youberg, A. M. (2019). Progress in simplifying hydrologic model parameterization for broad applications to post-wildfire flooding and debris flow hazards. *Earth Surface Processes and Landforms*, 44(15), 3078–3092. <https://doi.org/10.1002/esp.4697>
- Rengers, F. K., McGuire, L. A., Oakley, N. S., Kean, J. W., Staley, D. M., & Tang, H. (2020). Landslides after wildfire: Initiation, magnitude, and mobility. *Landslides*, 17, 2631–2641. <https://doi.org/10.1007/s10346-020-01506-3>
- Rengers, F. K., Tucker, G. E., Moody, J. A., & Ebel, B. A. (2016). Illuminating wildfire erosion and deposition patterns with repeat terrestrial lidar. *Journal of Geophysical Research: Earth Surface*, 121(3), 588–608. <https://doi.org/10.1002/2015JF003600>
- Richard, S. M., Clark, R., & Arrospeide, T. (2015). Geologic map of the southwestern part of the Tonto National Forest, Gila, Maricopa, Pinal and Yavapai Counties, Arizona. Arizona Geological Survey Digital Geologic Map, DGM-76 & DI-41, map scale 1:130,000. Retrieved from http://repository.azgs.gov/turi_gin/azgs/dlio/1615
- Robichaud, P., Wagenbrenner, J., Pierson, F., Spaeth, K., Ashmun, L., & Moffet, C. (2016). Infiltration and interrill erosion rates after a wildfire in western Montana, USA. *Catena*, 142, 77–88. <https://doi.org/10.1016/j.catena.2016.01.027>
- Rutter, A. J., Kershaw, K. A., Robins, P. C., & Morton, A. J. (1971). A predictive model of rainfall interception in forests. I. Derivation of the model from observations in a plantation of Corsican pine. *Agricultural Meteorology*, 9, 367–384. [https://doi.org/10.1016/0002-1571\(71\)90034-3](https://doi.org/10.1016/0002-1571(71)90034-3)
- Rutter, A. J., Morton, A. J., & Robins, P. C. (1975). A predictive model of rainfall interception in forests. II. Generalization of the model and comparison with observations in some coniferous and hardwood stands. *Journal of Applied Ecology*, 12(1), 367–380. <https://doi.org/10.2307/2401739>
- Schaap, M. G., Leij, F. J., & van Genuchten, M. T. (2001). Rosetta: A computer program for estimating soil hydraulic parameters with hierarchical pedotransfer functions. *Journal of Hydrology*, 251(3–4), 163–176. [https://doi.org/10.1016/S0022-1694\(01\)00466-8](https://doi.org/10.1016/S0022-1694(01)00466-8)
- Schmidt, K. M., Hanshaw, M. N., Howle, J. F., Kean, J. W., Staley, D. M., Stock, J. D., & Bawden, G. W. (2011). Hydrologic conditions and terrestrial laser scanning of post-fire debris flows in the San Gabriel Mountains, CA, U.S.A. In R. Genevois, D. L. Hamilton, & A. Prestininzi (Eds.), *Debris-flow hazards mitigation, mechanics, prediction, and assessment: Proceedings of 5th international conference on debris-flow hazards* (pp. 583–593). Casa Editrice University La Sapienza. <https://doi.org/10.4408/IJEGE.2011-03.B-064>
- Shakesby, R. A., Doerr, S. H. (2006). Wildfire as a hydrological and geomorphological agent. *Earth-Science Reviews*, 74(3–4), 269–307. <https://doi.org/10.1016/j.earscirev.2005.10.006>
- Sheridan, G. J., Lane, P. N. J., & Noske, P. J. (2007). Quantification of hillslope runoff and erosion processes before and after wildfire in a wet Eucalyptus forest. *Journal of Hydrology*, 343(1–2), 12–28. <https://doi.org/10.1016/j.jhydrol.2007.06.005>
- Shuttleworth, W. J. (1979). Evaporation. Institute of Hydrology, NERC, Report, 56. Retrieved from <https://arizona.pure.elsevier.com/en/publications/evaporation>
- Singleton, M. P., Thode, A. E., Sánchez Meador, A. J., & Iniguez, J. M. (2019). Increasing trends in high-severity fire in the southwestern USA from 1984 to 2015. *Forest Ecology and Management*, 433, 709–719. <https://doi.org/10.1016/j.foreco.2018.11.039>

- Smith, R. E., & Goodrich, D. C. (2000). Model for rainfall excess patterns on randomly heterogeneous areas. *Journal of Hydrologic Engineering*, 5(4), 355–362. [https://doi.org/10.1061/\(ASCE\)1084-0699\(2000\)5:4\(355\)](https://doi.org/10.1061/(ASCE)1084-0699(2000)5:4(355))
- Staley, D. M., Kean, J. W., Cannon, S. H., Schmidt, K. M., & Laber, J. L. (2013). Objective definition of rainfall intensity–duration thresholds for the initiation of post-fire debris flows in southern California. *Landslides*, 10(5), 547–562. <https://doi.org/10.1007/s10346-012-0341-9>
- Staley, D. M., Kean, J. W., & Rengers, F. K. (2020). The recurrence interval of post-fire debris flow generating rainfall in the southwestern United States. *Geomorphology*, 370, 107392. <https://doi.org/10.1016/j.geomorph.2020.107392>
- Staley, D. M., Negri, J. A., Kean, J. W., Laber, J. L., Tillery, A. C., & Youberg, A. M. (2017). Prediction of spatially explicit rainfall intensity–duration thresholds for post-fire debris flow generation in the western United States. *Geomorphology*, 278, 149–162. <https://doi.org/10.1016/j.geomorph.2016.10.019>
- Staley, D. M., Wasklewicz, T. A., & Kean, J. W. (2014). Characterizing the primary material sources and dominant erosional processes for post-fire debris flow initiation in a headwater basin using multi-temporal terrestrial laser scanning data. *Geomorphology*, 214, 324–338. <https://doi.org/10.1016/j.geomorph.2014.02.015>
- Stoof, C. R., Ferreira, A. J. D., Mol, W., van den Berg, J., De Kort, A., Drooger, S., et al. (2015). Soil surface changes increase runoff and erosion risk after a low-moderate severity fire. *Geoderma*, 239–240, 58–67. <https://doi.org/10.1016/j.geoderma.2014.09.020>
- Stoof, C. R., Vervoort, R. W., Iwema, J., van den Elsen, E., Ferreira, A. J. D., & Ritsema, C. J. (2012). Hydrological response of a small catchment burned by experimental fire. *Hydrology and Earth System Sciences*, 16(2), 267–285. <https://doi.org/10.5194/hess-16-267-2012>
- Tang, H., McGuire, L. A., Rengers, F. K., Kean, J., Staley, D. M., & Smith, J. B. (2019b). Developing and testing physically based triggering thresholds for runoff-generated debris flows. *Geophysical Research Letters*, 46(15), 8830–8839. <https://doi.org/10.1029/2019GL083623>
- Tang, H., McGuire, L. A., Rengers, F. K., Kean, J. W., Staley, D. M., & Smith, J. B. (2019a). Evolution of debris flow initiation mechanisms and sediment sources during a sequence of postwildfire rainstorms. *Journal of Geophysical Research: Earth Surface*, 124(6), 1572–1595. <https://doi.org/10.1029/2018JF004837>
- Thomas, M. A., Rengers, F. K., Kean, J. W., McGuire, L. A., Staley, D. M., Barnhart, K. R., & Ebel, B. A. (2021). Postwildfire soil-hydraulic recovery and the persistence of debris flow hazards. *Journal of Geophysical Research: Earth Surface*, 126(6), e2021JF006091. <https://doi.org/10.1029/2021JF006091>
- Thompson, S. E., Harman, C. J., Konings, A. G., Sivapalan, M., Neal, A., & Troch, P. A. (2011). Comparative hydrology across AmeriFlux sites: The variable roles of climate, vegetation, and groundwater. *Water Resources Research*, 47(10), W00J07. <https://doi.org/10.1029/2010WR009797>
- Tillery, A. C., & Rengers, F. K. (2020). Controls on debris-flow initiation on burned and unburned hillslopes during an exceptional rainstorm in southern New Mexico, USA. *Earth Surface Processes and Landforms*, 45(4), 1051–1066. <https://doi.org/10.1002/esp.4761>
- USDA Forest Service. (2020). BAER imagery support data download. Retrieved from <https://fsapps.nwcg.gov/baer/baer-imagery-support-data-download>
- Vandervaere, J.-P., Vauclin, M., & Elrick, D. E. (2000). Transient flow from tension infiltrometers II. Four methods to determine sorptivity and conductivity. *Soil Science Society of America Journal*, 64(4), 1272–1284. <https://doi.org/10.2136/sssaj2000.6441272x>
- Vieira, D. C. S., Fernández, C., Vega, J. A., & Keizer, J. J. (2015). Does soil burn severity affect the post-fire runoff and interrill erosion response? A review based on meta-analysis of field rainfall simulation data. *Journal of Hydrology*, 523, 452–464. <https://doi.org/10.1016/j.jhydrol.2015.01.071>
- Westerling, A. L., Hidalgo, H. G., Cayan, D. R., & Swetnam, T. W. (2006). Warming and earlier spring increase western U.S. forest wildfire activity. *Science*, 313(5789), 940–943. <https://doi.org/10.1126/science.1128834>
- Western Regional Climate Center. (2021). Reserve RS, New Mexico: Period of record monthly climate summary. Retrieved from <https://wrcc.dri.edu/cgi-bin/cliMAIN.pl?nm7386>
- Wieting, C., Ebel, B. A., & Singha, K. (2017). Quantifying the effects of wildfire on changes in soil properties by surface burning of soils from the Boulder Creek Critical Zone Observatory. *Journal of Hydrology: Regional Studies*, 13, 43–57. <https://doi.org/10.1016/j.ejrh.2017.07.006>
- Wittenberg, L., Malkinson, D., Beeri, O., Halutz, A., & Tesler, N. (2007). Spatial and temporal patterns of vegetation recovery following sequences of forest fires in a Mediterranean landscape, Mt. Carmel Israel. *Catena*, 71(1), 76–83. <https://doi.org/10.1016/j.catena.2006.10.007>
- Yerkes, R., & Campbell, R. (2005). *Preliminary geologic map of the Los Angeles 30' x 60' quadrangle, southern California*. U.S. Geological Survey Open-File Report 2005-1019. <https://doi.org/10.3133/ofr20051019>
- Zhang, R. (1997). Determination of soil sorptivity and hydraulic conductivity from the disk infiltrometer. *Soil Science Society of America Journal*, 61(4), 1024–1030. <https://doi.org/10.2136/sssaj1997.03615995006100040005x>